Harmful Algae
March 2022, Volume 113 Pages 102206 (13p.)
https://doi.org/10.1016/j.hal.2022.102206
https://archimer.ifremer.fr/doc/00752/86449/

Two toxigenic *Ostreopsis* species, *O.* cf. *ovata* and *O. siamensis* (Dinophyceae), from the South China Sea, tropical Western Pacific

Gu Haifeng [1, 2, *], Wang Yinuo [1, 2], Derrien Amelie [3], Hervé Fabienne [4], Wang Na [2], Pransilpa Mitila [5], Lim Po Teen [6], Leaw Chui Pin [6]

[1] School of Marine Sciences, Nanjing University of Information Science and Technology, Nanjing, 210044, China
[2] Third Institute of Oceanography, Ministry of Natural Resources, Xiamen 361005, China
[3] Ifremer, LER BO, Station de Biologie Marine, Place de la Croix, BP40537, F-29185 Concarneau CEDEX, France
[4] Ifremer (French Research Institute for Exploitation of the Sea), DYNECO, laboratoire Phycotoxines, rue de l'Ile d'Yeu, F-44311 Nantes Cedex 03, , France
[5] Department of Marine and Coastal Resources, East Gulf of Thailand, Rayong, Thailand
[6] Bachok Marine Research Station, Institute of Ocean and Earth Sciences, University of Malaya, 16310 Bachok, Kelantan, Malaysia

* Corresponding authors : Haifeng Gu, email address : guhaifeng@tio.org.cn ; Chui Pin Leaw, email address : cpleaw@um.edu.my

Abstract :

In the dinophyte genus Ostreopsis, seven out of 11 described species are known to produce various toxic compounds that were characterized in the palytoxins family. Species in the genus shared identical thecal plate patterns but differed in size, shape, and thecal plate ornamentation. Two species, O. cf. ovata and O. siamensis, have been reported from the Western Pacific, but information on toxin production is scarce. Here, we established nine strains of Ostreopsis from six localities in the South China Sea (SCS), covering the Gulf of Thailand, northern SCS (Hainan Island, Beibu Bay), and southern SCS (Peninsular Malaysia). Their morphology was examined by light and electron microscopy and the molecular phylogeny was inferred based on the LSU rDNA (D1-D3) and ITS rDNA sequences using maximum likelihood and Bayesian inference. Both O. cf. ovata and O. siamensis, albeit morphologically closely related, can be distinguished by a feature of the thecal pores with pronounced ridges in the latter. Molecular data further supported their species identity. Toxin production in the strains was examined by LC-MS/MS. O. cf. ovata strain T5PRBost02 was observed to produce Ovatoxin-k and Ovatoxin-j2 only; while Ostreocin-B and Ostreocin-D was produced by O. siamensis strain T10PRBost04. This is the first report confirming the production of palytoxins analogs in Ostreopsis species from the region.

Highlights

► *Ostreopsis siamensis* identified from waters of Peninsular Malaysia found to produce Ostreocin-B and Ostreocin-D. ► Two clades of *Ostreopsis* cf. *ovata* (A and B) were identified in the South China Sea. ► *Ostreopsis* cf. *ovata* clade A produces Ovatoxin k and j2, but clade B is nontoxic.

Keywords : BHAB, Dinoflagellates, Genetics, Morphology, Ostreopsis, Ovatoxins, Ostreocin

1. Introduction

Some species in the genus *Ostreopsis* Johs. Schmidt are known to produce toxic compounds which are chemical analogues of palytoxin (PlTX), the most potent marine biotoxins (Ciminiello et al., 2010; Ramos and Vasconcelos, 2010; García-Altares et al., 2015; Gladan et al., 2019). In the Mediterranean coasts, different ovatoxins (OVTXs) and isobaric PlTX have been reported in mussels, sea urchins and omnivorous or herbivorous fish (Alligizaki et al., 2008; Tubaro et al., 2011; Amzil et al., 2012; Bire et al., 2013; 2015), and ovatoxins can be aerosolized and dispersed in the air (Ciminiello et al. 2014; Medina-Pérez et al 2020). For the past two decades, *Ostreopsis* species have been reported to form massive high-biomass blooms in some coastal areas, particularly in the Mediterranean and Brazilian beaches, causing deleterious impacts to the marine ecosystems, human health, and the socio-economy (Pavaux et al., 2020 and references there in).

The dinophyte genus *Ostreopsis* was established a century ago (Schmidt, 1901), with the type species *O. siamensis* Johs. Schmidt described from plankton samples collected using a fine silk net near the Chang Islands, the Gulf of Thailand (Schmidt, 1901). However, in the recent past, many of the species have been described as epiphytes that inhabited benthic substrates such as sands and macroalgae (e.g., Faust et al., 1996; Leaw et al., 2001). The genus currently consists of 11 formally accepted species (Guiry and Guiry, 2021). They were delimited based on the subtle morphological distinction in cell size, shape, and the ornamentation of thecal plates (Fukuyo, 1981; Quod 1994; Faust and Morton, 1995; Faust et al., 1996; Faust, 1999),

while some recently described species were delineated with the inclusion of molecular genetic information (Accoroni et al., 2016; Verma et al., 2016). Nonetheless, the taxonomy of some species in the genus remains elusive, as classical taxonomic identification is difficult to distinguish among morphologically plastic species (Parson et al., 2012; Berdalet et al., 2017), and in some instances, they lack genetic information for comparison. For many years, most studies conferred their studied species as either *O*. cf. *ovata* (for smaller cells) or *O*. cf. *siamensis* (for bigger cells) (e.g., Penna et al., 2005, 2010; Accoroni et al., 2016; Zhang et al., 2018; Tibiriçá et al., 2019). With the advancement of molecular approach and the expansion of genetic data of the nuclear-encoded LSU rDNA and the internal transcribed spacers (ITS) region (Leaw et al., 2001; Penna et al., 2005, 2010; Sato et al., 2011; Tawong et al., 2014; Chomérat et al., 2019, 2020), some novel phylogenetic clades with distinct ribotypes have been recovered for *Ostreopsis*, of which the ribotypes were designated as *Ostreopsis* sp. 1 to 8 (Sato et al., 2011), and lately *Ostreopsis* sp. 9 (= *O*. cf. *siamensis*; Nguyen-Ngoc et al., 2021). This allowed further taxonomic clarification and assignments of previously described species by integrating the genetic data: *O*. *lenticularis* Y.Fukuyo (= *Ostreopsis* sp. 5; Chomérat et al., 2019), *O*. *mascarenensis* Quod (Chomérat et al., 2020), and *O*. *siamensis* (= *Ostreopsis* sp. 6; Nguyen-Ngoc et al., 2021), as well as novel species descriptions such as *O*. *fattorussoi* Accoroni, Romagnoli & Totti (Accoroni et al., 2016) and *O*. *rhodesiae* Verma, Hoppenrath & S.A.Murray (Verma et al., 2016). Not all *Ostreopsis* species are unambiguously linked to distinct genetic sequence information, this included species that have been rarely

encountered in the literature, i.e., *O. marina* M.A.Faust, *O. belizeana* M.A.Faust, *O. caribbeana* M.A.Faust, *O. heptagona* D.R.Norris, J.W.Bomber & Balech, and *O. labens* M.A.Faust & S.L.Morton.

Among the many *Ostreopsis* species, *O. ovata* Y.Fukuyo was the most widely studied species worldwide. The species was first described from Ryukyu Island, Japan, where it was distinguished morphologically from *O. siamensis* and *O. lenticularis* by its relatively smaller cell size and ovoid shape (Fukuyo, 1981). It has been reportedly found in French Polynesia, New Caledonia, the Caribbean Sea, the Tyrrhenian Sea, Reunion Island, the South China Sea, the western Mediterranean Sea, South Korea, and Brazil (Fukuyo, 1981, Besada et al., 1982; Tognetto et al., 1995; Faust et al., 1996; Leaw et al., 2001; Penna et al., 2005; Aligizaki and Nikolaidis, 2006; Mohammad-Noor et al., 2007; Kang et al., 2013; Carnicer et al., 2015; Gómez et al., 2017; Zhang et al., 2018). Although extensive assessment of the genetic diversity has been undertaken, no studies have referred the species to either of the genetic lineages. But rather, a distinct genetic lineage comprised of smaller-cells *Ostreopsis* was assigned as *O.* cf. *ovata* (reference herein) to confer *O. ovata sensu* Fukuyo (Fukuyo, 1981).

Despite its wide global distribution, only strains of *O.* cf. *ovata* from Japan, Brazil and the Mediterranean Sea have been reported to produce the palytoxin analogs, ovatoxins (Honsell et al., 2011; Nascimento et al., 2012; Suzuki et al., 2012; Tartaglione et al., 2017; Tibiriçá et al., 2019). These strains appear to be genetically distinct from those reported from the Western Pacific as revealed by the molecular

phylogenetic inferences of some previous studies (Penna et al., 2005, 2010; Tibiriçá et al., 2019), but whether *O*. cf. *ovata* strains from the South China Sea are toxic remained unclear.

This study aims to (1) fully understand the genetic diversity of *O.* cf. *ovata* and *O. siamensis* in the South China Sea; (2) investigate the toxin production potential of *O.* cf. *ovata* and *O. siamensis* in this region. Nine strains of *Ostreopsis* were established from three distant localities in the South China Sea, covering the Gulf of Thailand, northern and southern parts of the Sea (Fig. 1). Strains established were undergone detailed morphological examination using light and scanning, and transmission electron microscopy. The phylogenetic relationships of the species found in this study were inferred from the newly generated nucleotide sequence data of the nuclear-encoded rDNA in the LSU D1-D3 and the ITS regions. Toxicity in six strains of *Ostreopsis* was analyzed using liquid chromatography coupled with tandem mass spectrometry (LC-MS/MS).

2. Materials and methods

2.1. Sample collection and treatment

Sampling for benthic substrates was undertaken at Hainan Island, Weizhou Island, China, and Rawa Island, Terengganu, Malaysia (Fig. 1) between 2015 and 2018. Sand samples were collected from seabed by scuba divers and placed into bottles containing seawater from the same location. The samples were stirred vigorously to detach the epibenthic cells and the suspension settled in a polycarbonate

bottle. The settled material was rinsed with filtered seawater and transferred into a petri dish. Single *Ostreopsis* cells were isolated with a finely drawn micropipette using an Eclipse TS100 inverted microscope (Nikon, Tokyo, Japan). Eight strains of *Ostreopsis*, *viz*. TIO15, TIO25, TIO121, TIO123, TIO912, T5PRBost02, OsPR08N, and T10PRBost04 (Table 1), were established from the sand samples. An attempt to collect *Ostreopsis* cells from plankton samples were undertaken at Mak Island, the Gulf of Thailand (Fig. 1), using a 10 μm mesh-size plankton net on November 17, 2017. A strain TIO897 was established from the plankton sample. All strains were maintained in f/2-Si medium (Guillard and Ryther, 1962) with a salinity of 30 at 25 ℃, 90 $\mu E \cdot m^{-2} \cdot s^{-1}$ under a 12:12 h light: dark cycle.

2.2. Morphological observation of motile cells with LM and SEM

Live cells were examined and photographed using a Zeiss Axio Imager light microscope (LM, Carl Zeiss, Göttingen, Germany) equipped with a Zeiss Axiocam HRc digital camera. The size of a minimum of 30 cells was measured using Axiovision v.4.8.2 software at 400× magnification. To observe the shape and location of the nucleus, cells were stained with 1:100,000 SYBR Green (Sigma Aldrich, St. Louis, USA) for 1 min, and photographed using the Zeiss fluorescence microscope with a Zeiss-38 filter set (excitation BP 470/40, beam splitter FT 495, emission BP 525/50). Chloroplast autofluorescence was observed on live cells using the above-mentioned microscope equipped with a Chroma filter cube (emission filter ET480/20x, dichromatic mirror AT505dc, suppression filter AT515lp), and digitally

photographed using a Zeiss Axiocam HRc digital camera. Calcofluor white was used to discern thecal plates in vegetative cells following the method of Fritz and Triemer (1985).

For scanning electron microscopy (SEM), the mid-exponential batch cultures were concentrated by a Universal 320 R centrifuge (Hettich-Zentrifugen, Tuttlingen, Germany) at 850 *g* for 10 min at room temperature. Cells were fixed with 2.5% glutaraldehyde for 3 h at 8 ℃, rinsed with Milli-Q water twice and post-fixed with 1% OsO_4 overnight at 8 ℃ in a tube. The supernatant was removed, and the settled cells were transferred to a coverslip coated with poly-L-lysine (molecular weight 70,000–150,000). The cells attached to the cover slip were rinsed with Milli-Q water twice. The samples were then dehydrated in a graded ethanol series (10, 30, 50, 70, 90 and 3× in 100%, 10 min at each step), critical point dried using a K850 Critical Point Dryer (Quorum/Emitech, West Sussex, UK), sputter-coated with gold, and examined with a Zeiss Sigma FE scanning electron microscope (Carl Zeiss, Oberkochen, Germany). Labelling of thecal plate tabulation follows a modified Kofoidian system (cf. Fensome et al., 1993), and the sulcal plates were labeled according to Balech (1980).

For transmission electron microscopy (TEM), mid-exponential batch cultures of strain TIO897 was fixed in 2.5% glutaraldehyde in phosphate buffer saline (PBS, 0.1 M, pH 7.4) for 1 h, concentrated by centrifugation and then washed three times in PBS for 10 min each. Samples were then post-fixed in 1% OsO_4 overnight at 4 °C and subsequently washed in PBS (3×, 10 min each). The cells were then dehydrated

through a graded ethanol series (10, 30, 50, 70, 95, 3× in 100%, 10 min each). The pellet was embedded in a Spurr's resin (Spurr, 1969) and sectioned with a Reichert Ultracut E microtome (Leica, Vienna, Austria). The thin sections were mounted on Formvar-coated grids, stained with uranyl acetate and lead citrate, and observed in a JEOL JEM-100 transmission electron microscope (JEOL, Tokyo, Japan).

2.3. Gene amplification and sequencing

The genomic DNA from each strain was extracted from 10 mL of exponentially growing cultures using a MiniBEST Universal DNA Extraction Kit (Takara, Tokyo, Japan) according to the manufacturer's protocol. Gene amplifications were carried out in a 50 μL reaction containing 1×PCR buffer, 50 μM dNTP mixture, 0.2 μM of each primer, 10 ng of template genomic DNA, and 1 U of ExTaq DNA Polymerase (Takara, Tokyo, Japan). The LSU rDNA (D1-D3) was amplified using the primer pair D1R/28 and 1483R (Daugbjerg et al., 2000), while the ITS region (ITS1–5.8S–ITS2) was amplified using ITSA and ITSB (Adachi et al., 1996). The polymerase chain reaction was performed using a Mastercycler (Eppendorf, Hamburg, Germany) with the thermal cycling procedure of 4 min at 94 ℃, followed by 30 cycles of 1 min at 94 ℃, 1 min at 45 ℃, 1 min at 72 ℃, and final extension of 7 min at 72 ℃. The amplicons were purified using a SanPrep Column DNA Gel Extraction Kit (Sangon Biotech, Shanghai, China) and sequenced directly in both directions on an ABI PRISM 3730XL (Applied Biosystems, Foster City, CA, USA) following the manufacturer's instructions.

Direct sequencing of LSU rDNA and ITS region yielded heterozygous sequences for strain TIO897 and T10PRBost04, thus the amplicons were cloned into a pUCm-T vector and a total of ten clones were selected and sequenced. All newly obtained sequences were deposited in GenBank (NCBI) with accession numbers OM514336 to OM514347 and OM513966 to OM513975.

2.4. Sequence alignment and phylogenetic analysis

Newly obtained sequences of LSU rDNA (D1–D3) and ITS region were incorporated into systematically representative datasets of *Ostreopsis* sequences that were retrieved from the GenBank nucleotide database (NCBI). The nucleotide sequences were aligned using MAFFT v7.110 (Katoh and Standley, 2013; http://mafft.cbrc.jp/alignment/server/) with the default settings. The multiple alignments were manually checked for potential errors using BioEdit v. 7.0.5 (Hall, 1999).

For Bayesian inference (BI), jModelTest (Posada, 2008) was used to select the most appropriate model of molecular evolution with Akaike Information Criterion (AIC) excluding invariable sites (+I). Bayesian reconstruction of the data matrix was performed using MrBayes 3.2 (Ronquist and Huelsenbeck, 2003) with the best-fitting substitution model (GTR+G). Four Markov chain Monte Carlo (MCMC) chains were performed for 4,000,000 generations, sampling every 100 generations. Convergence diagnostics were graphically estimated as in Nylander et al. (2008) and the first 10% of burn-in trees were discarded. A majority rule consensus tree was reconstructed to

examine the posterior probabilities of each clade. Maximum likelihood (ML) was performed using RaxML v.7.2.6 (Stamatakis, 2006) on the T-REX web server (Boc et al., 2012) using the GTR+G model. Node support was assessed with 1000 bootstrap replications. The ITS dataset was used to estimate divergence rates using PAUP*4b10 (Swofford, 2002) by constructing the uncorrected pairwise (*p*) distance matrices.

2.5. Toxin analysis

At stationary phase about 10^5 – 10^6 cells for one strain of *O. siamensis* and five strains of *O.* cf. *ovata* were collected by centrifugation in 2 mL microcentrifuge tubes and stored at -20 °C. For the extraction, 300 µL of methanol were added to the cell pellets and the mixture was transferred in a 1.5 mL Safelock Eppendorf tubes. Glass beads (100–250 µm in diameter) were added before cell lysis using a Mixer Mill equipment (MM400, Retsch) at 30 Hz for at least 80 min. After centrifugation at 15000 *g*, the supernatant was ultrafiltered (0.2 µm, Nanosep MF, Pall).

Sample analyses were performed by LC-MS/MS using a Shimadzu UFLCxr system coupled to a triple quadruple hybrid mass spectrometer Q-Trap (API400QTrap, Sciex) equipped with a heated electrospray ionization (ESI) source as detailed in Chomérat et al. (2019). The LC-MS/MS methods were used to detect 20 toxins (Table S1). The ESI interface operated using the following parameters: curtain gas 20 psi, temperature: 300 °C, gas1 40 psi; gas2 40 psi, ion spray voltage 5500 V. The dwell time was 90 ms. The transitions and MS/MS parameters that were used for the MRM mode are reported in table S1. Quantification was performed relative to a palytoxin

standard (Wako Chemicals GmbH) with a 6-point calibration curve. The limit of quantification was 30 ng mL^{-1} for the palytoxin standard.

In addition to low resolution LC-MS/MS targeted analyses, samples analyses were performed by UPLC-HRMS (High Resolution Mass Spectrometry) using an Agilent UHPLC 1290 Infinity II system coupled to a QTOF mass spectrometer (QTOF 6550, Agilent) equipped with a Dual Jet Stream electrospray ionization (ESI) interface. The chromatographic conditions are the same as for the low resolution analysis, with minor modifications (flow rate: 0.4 ml/min and oven: 30°C). The mass spectra were recorded in full scan over a mass range [100-2800] (2 spectra per second) to confirm the ion species characteristic of OVTXs, as previously did for ostreocins (Chomérat et al 2020). A calibration check was performed continuously over the entire run time using reference masses *m/z* 121.0509 and *m/z* 922.0099.

3. Results

3.1. Morphological characterization

In this study, nine strains of *Ostreopsis* were established, eight were identified as *O*. cf. *ovata* and one was identical to *O*. *siamensis*. *Ostreopsis* cf. *ovata* were found in the sand samples collected from China and Malaysia, and in plankton samples collected from Thailand, while *O*. *siamensis* was found in Rawa Island, Malaysia as epiphytes (Table 1).

3.1.1. Ostreopsis cf. *ovata*

All strains of *O.* cf. *ovata* displayed indistinguishable morphological features when observed under light and epifluorescence microscopy (Fig. 2). In general, cells are broadly oval and lenticular. Chloroplasts were radially arranged. The oval nucleus is small and located posteriorly (Fig. 2).

Cells of strain TIO897 from Thailand were 39.0–58.9 μm (50.1 ± 4.5 μm, *n* = 36) in dorsoventral length (DV) and 29.6–50.3 μm (39.7 ± 5.0 μm, *n* = 36) in cell width (W), with a mean DV/W ratio of 1.28 ± 0.09 (1.08–1.43; *n* = 36). Cell size of strain TIO123 from China ranged from 46.0 to 59.5 μm (52.3 ± 3.5 μm, *n* = 50) in dorsoventral length and 31.0–44.5 μm (36.4 ± 3.2 μm, *n* = 50) wide, with a mean DV/W ratio of 1.44 ± 0.10 (1.23–1.70; *n* = 50). Size range of strain OsPR08N from Malaysia was relatively smaller, ranging from 28.7 to 37.9 μm (33.0 ± 3.0 μm, *n* = 10) in dorsoventral length and 17.7–28.7 μm (24.5 ± 3.9 μm, *n* = 10) wide. The mean DV/W ratio was 1.39 ± 0.33 (0.97–2.00; *n* = 10).

Detailed morphological observations of strain TIO879 from Thailand are shown in Figs 2 and 3. Cells were broadly oval in apical and antapical views. The cells were biconvex, and flattened, with the cingulum mimicking a sine curve in the ventral and lateral views (Fig. 2A). The thecal plate pattern was Po, 3′, 7″, 6c, 6s, 5‴, 2⁗ (Figs 2E–F, 3B–D). The apical pore complex (APC) consisted of a narrow, elongated and slightly curved pore plate (Po) bearing a slit and two rows of pores (Fig. 3E, F). The Po inside the APC contained 10–16 pores on the dorsal side (14 ± 2, *n* = 11) and nine pores on the ventral side in two examined cells (Fig. 3E, F). The APC

was located parallel to the left mid-lateral to dorsal cell margin. The first apical plate (1′) was elongated, located mostly on the left side of the cell (Figs 2E, 3B). On its dorsal part, it slightly protruded over the APC (Fig. 3B). The second apical plate (2′) was narrow and elongated, and located below the APC, extending dorsally to the Po plate, and reaching about the whole plate 3′ to contact plate 4″ (Fig. 2E). The third apical plate (3′) was six-sided in shape, in contact with plates 1′, 2′, 4″, 5″ and 6″, but had a very short suture with the Po (Fig. 3B). In the precingular series, plates 1″ and 4″ were smaller while plates 2″ and 6″ were larger (Fig. 2E). All precingular plates were four-sided except plates 2″ and 6″, which were five-sided (Figs 2E, 3B). The postcingular plate series comprised of five plates (Figs 2F, 3C); plate 1‴ was small and was more visible in the ventral view than in the antapical view (Fig. 2F). The remaining four postcingular plates were large (Fig. 2F). Of the postcingular plates, plate 1‴ was three-sided, plate 2‴ was five-sided, and plates 3‴, 4‴ and 5‴ were four-sided (Figs 2F, 3C).

The two antapical plates were unequal in size; plate 1⁗ was relatively small and in contact with the left side of the posterior sulcal plate (Sp) and the right anterior sulcal plate (Sda), while plate 2⁗ was elongated, sutured plates 2‴ and 5‴, almost parallel (Fig. 3C). The cingulum consisted of six distinct plates. The ventral pore (Vo) was located within the anterior sulcal plate (Sa). The cell surface was smooth, covered by round pores of 0.19–0.31 μm in diameter (0.26 ± 0.03 μm, n = 50) and scattered all over the plates (Fig. 3B). Small pores with diameters of approximately 0.10 μm were observed but very rare.

Six sulcal plates were observed (Fig. 3D): Sa, Sda, the left anterior sulcal plate (Ssa), the right posterior sulcal plate (Sdp), the left posterior sulcal plate (Ssp), and Sp. The round Sa contacted the plates 1″, 7″, Sda, and Ssa. The Ssa and Sda plates were similar in size and much larger than the other sulcal plates. Plate Sp touched the plates 5‴, 1⁗, Sdp, Sda, and 2⁗. Cell morphology of strain TIO123 from China was indistinguishable from strain TIO897 (Supplementary Material Fig. S1).

Longitudinal sections of strain TIO897 cells showed an oval nucleus situated posteriorly, many radially arranged chloroplasts, several large and dark lipid bodies, and numerous small starch bodies (Fig. 4A–C). The thylakoids were grouped in two or three rows to form lamellae (Fig. 4D). The chloroplasts were enveloped by three membranes. The nucleus contained condensed chromosomes and an irregular nuclesome (Fig. 4E). Both trichocysts and mucocysts were present. The mucus canal was 1.8–3.8 μm long and 0.4–0.5 μm wide and was surrounded by numerous mucocysts. The mucus canal had three membranes and numerous fibrils along the inner membrane (Fig. 4F).

3.1.2. Ostreopsis siamensis

Cells of strain T10PRBost04 from Malaysia were broadly oval in apical and antapical views. The cells were biconvex, and flattened, with the cingulum mimicking a sine curve in the ventral and lateral view (Fig. 5A). Cells were 44.7–73.4 μm in dorsoventral length (55.2 ± 6.6 μm, n = 37) and 31.4–57.5 μm (44.5 ± 6.3 μm, n = 37) wide. The mean DV/W ratio was 1.25 ± 0.12 (1.09–1.60; n = 37).

The thecal plate pattern was Po, 3′, 7″, 6c, 6s, 5‴, 2⁗. The APC consisted of a narrow, elongated and slightly curved Po bearing a slit and two rows of pores (Fig. 5C). The Po inside the APC contained 15 pores on the dorsal side and 13 pores on the ventral side in an examined cell (Fig. 5C). The APC was located parallel to the left mid-lateral to dorsal cell margin. Plate 1′ was elongated, located mostly on the left side of the cell (Fig. 5B). Plate 2′ was narrow and elongated, and located below the APC, extending dorsally to the Po plate, and reaching about the whole plate 3′ to contact plate 4″ (Fig. 5B, C). Plate 3′ was six-sided in shape, was in contact with plates 1′, 2′, 4″, 5″ and 6″ but also had a very short suture with the Po plate (Fig. 5B, C). In the precingular series, plates 1″ and 4″ were smaller while plates 2″ and 6″ were larger (Fig. 5B). All precingular plates were four-sided except for plates 2″ and 6″ which were five-sided. The postcingular plate series comprised five plates (Fig. 5D); plate 1‴ was small and was more visible in the ventral view than in the antapical view (Fig. 5E). The remaining four postcingular plates were large (Fig. 5D).

The two antapical plates were unequal in size; plate 1⁗ was relatively small and in contact with the left side of Sp and Sda, while plate 2⁗ was elongated and sutured with plates 2‴ and 5‴, almost parallel (Fig. 5D, E). The cingulum consisted of six distinct plates (Fig. 5F). The ventral pore (Vo) was located within Sa. The cell surface was smooth, covered by round pores of 0.36–0.55 μm in diameter (0.41 ± 0.05 μm, n = 30) with a pronounced rim (Fig. 5B). Smaller pores without a rim were occasionally observed with diameters of approximately 0.30 μm. Five sulcal plates were identified (Fig. 5E): Sa, Sda, Ssa, Sdp, and Sp.

3.2. Molecular characterization

3.2.1. LSU rDNA (D1–D3) phylogeny

In the LSU rDNA dataset, the Malaysian *O.* cf. *ovata* strain OsPR08N differed from the Thai strain TIO897 at five nucleotide positions (99.64% similarity). The Chinese strains (TIO15, TIO25, TIO121, TIO123, and TIO912) differed from each other at only one position, sharing 97.25% and 96.38% similarity with strains TIO897 and T5PRBost02, respectively. The two clones of *O. siamensis* strain T10PRBost04 shared 98.44% similarity. Clone A shared 97.47% similarity with strain PNA19-9 from French Polynesia (GenBank accession number: MT183170), 94.34% and 91.66% similarity with strain NT013 from Vietnam (GenBank accession number: JX065570), and strain OA21 from Japan (GenBank accession number: AB605828), respectively.

The phylogenetic analyses of LSU rDNA (D1–D3) yielded identical tree topologies by ML and BI; with the ML tree shown in Fig. 6. The resulting trees revealed distinct end-clades comprised of taxa of previously defined species, *O. siamensis*, *O. lenticularis*, *O. rhodesiae*, *O. fattorussoi*, *O. mascarenensis*, *O.* cf. *ovata*, and four ribotypes, *Ostreopsis* sp. 1, sp. 2, sp. 7, and sp. 8.

The end-clade of *O.* cf. *ovata* was monophyletic, supporting by strong nodal supports (ML/BI, 98%/0.81), which formed a sister group to *Ostreopsis* sp. 1. Taxa in *O.* cf. *ovata* were divided into two clades that were supported by maxima nodal supports (ML/BI, 100%/1.0). Here, the clades were referred as Clade A and Clade B

(Fig. 6). Clade A comprised of strains with geographically diverse origin, this included strains from Western Pacific (Malaysia, Hong Kong, and Japan), Western Atlantic (Belize, Brazil), Eastern Atlantic and the Mediterranean Sea; while Clade B comprised of strains mainly from the Western Pacific (Thailand, Malaysia, Vietnam, Indonesia, China, and Australia) except a strain from Belize (Western Atlantic).

As of strain T10PRBost04 (Malaysia), the phylogenetic inferences consistently placed the strain with other taxa in the *O. siamensis* lineage (= *Ostreopsis* sp. 6, cf. Sato et al., 2011) (Fig. 6). Intragenomic variability of the strain was low (98.4% similarity); while the intraspecific divergences among the *O. siamensis* strains ranged from 91.7% to 97.5% similarity.

3.2.2. ITS dataset and phylogeny

In the ITS dataset, pairwise genetic distances in *O. siamensis* strains ranged from 0.01 to 0.14 and in *O.* cf. *ovata* ranged from 0.01 to 0.14 too (Table 2). The *O.* cf. *ovata* strains TIO15, TIO25, TIO121, TIO123, and TIO912 differed from each other at only one position in the ITS region, but significant heterogeneity was detected with strain TIO897 from Thailand (90.5% similarity). Likewise, considerable high sequence heterogeneity was observed between the two Malaysian strains OsPR08N and T5PRBost02, with sequence similarity of only 83.9%. As of strain T10PRBost04, it shared 92.0% similarity with *O. siamensis* strain VNPR009 from Vietnam (MT968508), and 76.4% with strain IR33 from Japan (AB674920).

The analyses of ML and BI derived from the ITS dataset yielded identical phylogenetic trees, with the ML tree illustrated in Fig. 7. The phylogenetic trees consistently revealed 11 well resolved monophyletic clades (*O. mascarenensis*, *O. siamensis*, *O. lenticularis*, *O. rhodesiae*, *O. fattorussoi*, *O*. cf. *ovata*, and *Ostreopsis* sp. 1–4, 7, and 8).

The end-clade of *O*. cf. *ovata* was monophyletic, strongly supported by ML (bootstrap value of 97%). The end-clade, like in the LSU topology, formed two strongly supported clades: Clade A and Clade B (Fig. 7). The Malaysian strain T5PRBost02 clustered with other strains from Japan, Hong Kong, Brazil and the Mediterranean in Clade A, supported with the strong nodal supports by ML and BI (100%/0.99). Two groups were resolved in Clade B with strong ML bootstrap support (92%), forming subclades B1 and B2. The strains TIO897 (Thailand) and OsPR08N (Malaysia) were clustered in subclade B1 together with strains from Malaysia, Thailand, Australia, Reunion Island, and China (ML/BI, 100%/0.99). The Chinese strains (TIO15, TIO25, TIO121, TIO123, and TIO912) were grouped in subclade B2 with those from Thailand, Belize, Ecuador, Guadeloupe, Indonesia, and Malaysia (ML/BI, 95%/0.82).

3.3. Toxin compounds in Ostreopsis

Neither palytoxin nor ovatoxins were detected in the four *O*. cf. *ovata* strains from clade B (Table 1). However, Ovatoxin-k (0.46 to 0.82 pg/cell) and

Ovatoxin-j1/j2 (1.57 to 4.83 pg/cell) were detected in the *O.* cf *ovata* strain T5PRBost02 (clade A). Ostreocin-B (0.27 to 1.54 pg/cell) and Ostreocin-D (0.32 to 2.14 pg/cell) were detected in the *O. siamensis* strain T10PRBost04. The percentage of Ostreocin-D is thus 56% on average in the strain. As no standard is commercially available for these toxins, identifications were confirmed by high resolution mass spectrometry. Exact masses obtained by HRMS analyses confirmed the presence of Ovatoxin-k (Δ ppm: -5.0 to -1.1) and Ovatoxin-j1/j2 (Δ ppm: -4.7 to 0) in the strain T5PRBost02 (Supplementary Material Fig. S2). In our analysis, the chromatographic peak of Ovatoxin j1/j2 is more retain than Ovatoxin-k, so, according Tartaglione et al., 2016, we can suggest we have the Ovatoxin-j2 in our sample. HRMS analyses also confirmed the presence of Ostreocin-B (Δ ppm: -4.9 to -1.1) and Ostreocin-D (Δ ppm: -4.9 to +2.5) in the *O. siamensis* strain T10PRBost04 (Supplementary Material Fig. S3).

4. Discussion

Although only a small portion of the South China Sea has been sampled in this study, even so, there is no disputing that toxigenic *Ostreopsis* species occur in the region. Many studies have documented the occurrences of some *Ostreopsis* species from the waters (e.g., Leaw et al., 2001; Mohammad-Noor et al., 2007; Tawong et al., 2014; Zhang et al., 2018), but information on the toxicity or toxin production potential was scant. Here, we provided detailed morphology and molecular information, as well as the toxin production of two toxigenic *Ostreopsis* species, *O*. cf. *ovata* and *O. siamensis*, from the South China Sea.

Many past studies have substantiated that the genus *Ostreopsis* exhibited high species diversity, with the presence of many unrecognized lineages in the molecular phylogeny (e.g., Penna et al., 2010; Sato et al., 2011; Rhodes et al., 2017). The taxonomic progress, however, has been impeded by the high degree of morphological plasticity and similarity among species. Morphospecies concept in the genus *Ostreopsis* is often challenging, as species displayed little informative diagnostic features, and are morphologically alike. As a case in point, the traits of cell sizes and shapes that were often used to delineate among species of *Ostreopsis*. *Ostreopsis siamensis* was originally described with the cell size of 90 µm long (Schmidt 1901); later, it was reported with varying size ranges (60–100 µm, Fukuyo, 1981; 58.0–82.5 µm, Chomérat et al., 2020; 46–92 µm, Nguyen-Ngoc et al., 2021). The *O. siamensis* strain from Malaysia in this study, however, was much smaller (31.4–57.5 µm) than those previously reported, suggesting that cell size alone is not informative in

distinguishing species, such as *O. ovata sensu* Fukuyo (Fukuyo, 1981) and *O. siamensis*. For many years, numerous studies have conferred their species under study as either *O.* cf. *ovata* for smaller cells or *O.* cf. *siamensis* for bigger cells (e.g., Penna et al., 2005, 2010; Accoroni et al., 2016; Zhang et al., 2018; Tibiriçá et al., 2019). In addition, some cells of *O. siamensis* in culture in this study appear broadly ovoid to ovate, while cells were round and oyster-shaped as described in the original descriptions of *O. siamensis* (Schmidt, 1901). This indicated that the character of cell shape too, is not a good indicator in delimiting species of *Ostreopsis*.

Contrarily, the features of thecal pores (i.e., number of pores, sizes, and shape) have been considered useful in differentiating among *Ostreopsis* species. For example, *O. lenticularis* was distinguished from its closely related species *O. siamensis* by the presence of two sizes of thecal pores as observed under LM (Fukuyo, 1981), this was later confirmed by the observations using high-resolution SEM (Chomérat et al., 2019). Cells of *O. siamensis* from Malaysia possessed equal large-size pores with pronounced rims, this character was also consistently observed in *O. siamensis* cells from Vietnam and South Ocean (Chomérat et al., 2020; Nguyen-Ngoc et al., 2021). This character (pores with rim), however, was not observed in *O. ovata* (Fukuyo, 1981; Leaw et al., 2001) nor *O.* cf. *ovata* (Penna et al., 2005; Zhang et al., 2018; Tibiriçá et al., 2019). Verma et al. (2016) designated the cells from the temperate southeast Australia as *O.* cf. *siamensis*, but the thecal pores were without pronounced rims; as pointed out by other studies, the species is in need of revision and is likely belonged to a new species (Chomérat et al., 2020; Nguyen-Ngoc et al., 2021).

Similarly, the Mediterranean *O.* cf. *siamensis* reported by Penna et al. (2005) and David et al. (2013) also lacks thecal pores with rims. Likewise, *O. siamensis* that reported in Faust (1996) from Japan and in Chang et al. (2000) from New Zealand were most likely misidentified as the pores were without rims. In contrast, cells of *O. labens* exhibited thecal pores with pronounced rims. This species was only described from Japan and Belize (Faust and Morton, 1995); no genetic data is available to assign the species to any one lineage, thus whether it is a junior synonym of *O. siamensis* remains to be determined.

According to the original descriptions of *O. siamensis* and *O. ovata*, both have a short plate 2′, which does not extend to contact plate 4″ (Schmidt, 1901; Fukuyo, 1981). This plate, however, is too small to be observed under LM, and thus has often been overlooked in the earlier studies. *Ostreopsis ovata* was described from Kabira Bay of Ishigaki Island, Okinawa, Japan (Fukuyo, 1981), but strains from the type locality have not been examined using contemporary methods that integrating molecular characterization. Therefore, strains resembling *O. ovata* (cf. Fukuyo, 1981) is often referred as *O.* cf. *ovata* (references herein). It is not the purpose of this study to provide formal descriptions of *O. ovata*. The detailed morphology, as well as the ultrastructure of *O.* cf. *ovata* from the South China Sea, presented here further support the assessment that using morphology will not allow the assignment of the candidate species as *O. ovata* with confidence.

While confident morphological assignment of specimens to *O. ovata* is difficult, our results on the molecular phylogeny and many others (references herein)

supported a single lineage of *O*. cf. *ovata* by forming a strongly supported monophyletic clade in the phylogenetic trees. It is interesting to note that, with the newly generated sequences in our study, two well resolved clades, Clade A and Clade B, were revealed with strong nodal supports (see Figs 6, 7). Previous studies have clustered *O*. cf. *ovata* sub-clades based on the origin of strains, such as South China Sea (SCS), Malacca Strait, Mediterranean/Atlantic/Pacific oceans, and Thailand (Leaw et al., 2001; Penna et al., 2005; Tawong et al., 2014). The two clades however, as revealed in this study, were not congruent with biogeographical structuring (see Fig. 8), but the clading may imply evolutionary significance in term of the specific trait in toxin production (see discussion below). Nonetheless, strains from the two distinct clades examined in this study were identical in term of the outer morphology, confirming the previous findings of Zhang et al. (2018) and Tibiriçá et al. (2019).

The degree of genetic divergence was high among *O.* cf. *ovata* strains, with the divergence estimated <14% in the LSU dataset. The genetic distance was larger than that detected within *O. lenticularis* (<7%) (Chomérat et al., 2019), supporting the hypothesis that the two clades of *O.* cf. *ovata* are indeed a species complex. The strain kab013 that collected from the type locality of *O. ovata sensu* Fukuyo (Y. Fukuyo, personal communication to K. Mertens) falls within the *O.* cf. *ovata* clade A. Whether *O. ovata* could be assigned to one of the genetic lineages required more in-depth investigations of the specimens from the type locality.

It is interesting to note that *O.* cf. *ovata* clade A lineage, which are often found in the Atlantic (Brazil and Mediterranean Sea), was rarely found in the Western

Pacific; it has only been documented from Japan, Hong Kong, and Malaysia (Fig. 8). One of the arguments as to why it was seldom detected in the region is that the lineage was less dominant over another, and thus have escaped detection. In the South China Sea, taxa in the Clade B lineage have frequently been reported (Leaw et al., 2001; Tawong et al., 2014; Zhang et al., 2018; Nguyen-Ngoc et al., 2021), but the occurrence of taxa from Clade A was only confirmed until now. Furthermore, our previous results from the ITS2 metabarcoding data that obtained from the Gulf of Thailand and Perhentian Islands, Malaysia (Fu et al., 2021) showed that the proportion of the *O*. cf. *ovata* genetic lineages (Clade A:B) in the phytoplankton assemblages was in the ratio of 1:360, further supported the notion that Clade A lineage is rare in the region. Previous field investigations in the Perhentian Islands by Yong et al. (2018) and Lee et al. (2020) had demonstrated temporal distribution and abundance of *Ostreopsis* spp. in a tropical reef system, but unlike the bloom events in the Mediterranean (as reviewed in Pavaux et al., 2020), no cases of Ostreopsis-related respiratory irritations in humans have been reported thus far, likely due to the relatively low biomass of *Ostreopsis* ($< 3.4 \times 10^4$ cells 100 cm^{-2}; Yong et al., 2018) as compared to the bloom densities in the Mediterranean coasts ($> 10^6$ cells g^{-1}, e.g., Brescianini et al., 2006; Totti et al., 2010). It is difficult to compare cell concentrations expressed per surface (using artificial substrates) with epiphytic concentrations per gram of freshweight of macroalgae. However, as illustrated in Jauzein et al. 2018 (Fig. 3B), the 10^4 cells 100 cm^{-2} could correspond to 10^6 cells g^{-1}, which have been related to irritative symptoms. The key differences might be that

toxic *Ostreopsis* cells are not dominant in the Perhentian Islands. It has been demonstrated by some studies that blooms of *Ostreopsis* were largely regulated by seawater temperatures (e.g., Yong et al., 2018; Giussani et al., 2017), of which the blooms were more robust with warmer seawater temperatures. But it has been shown that toxicity and symptoms do not depend on seawater temperature but to complex physiological processes and physical processes favoring aerosolization of the toxic compounds (Vila et al., 2016; Medina-Pérez et al., 2020). By realizing the co-occurrences of potential toxigenic genetic entities, it is worthwhile to further investigate the bloom dynamics of *Ostreopsis* and its regulating factors to gain better insights on the underlying mechanism presiding *Ostreopsis* bloom dynamics.

Genetic divergence among *O. siamensis* strains, like *O.* cf. *ovata*, was high (14%), suggesting cryptic species diversity in the lineage. But unlike *O.* cf. *ovata*, *O. siamensis* has only been found in the Western Pacific (Asia and French Polynesia). New records of this species are expected in near future as the taxonomic identity and corresponding genetic lineage (= *Ostreopsis* sp. 6) have been clarified only recently (Chomérat et al., 2020; Nguyen-Ngoc et al., 2021).

In this study, none of the strains that grouped in the Clade B lineage produced ovatoxins; this finding agreed with that reported by Tawong et al. (2014) based on mouse bioassay. Furthermore, strain CAWD174 (Cook Island), which was also grouped in Clade B, did not produce the toxins (Rhodes, 2011). In contrast, only *O.* cf. *ovata* strain T5PRBost02 that was grouped in the Clade A lineage in this study produced ovatoxins. This finding is congruent with those studies reported from Brazil

and Mediterranean Sea, of which the *O*. cf. *ovata* strains were members in the Clade A lineage (Penna et al., 2005; Accoroni et al., 2011; Nascimento et al., 2012; Brissard et al., 2014; Tartaglione et al., 2017; Tibiriçá et al., 2019); this suggested that ovatoxins production in *O*. cf. *ovata* is an important distinctive trait, likely a genetically stable character, in the Clade A lineage.

It is noteworthy that the *O*. cf. *ovata* strains in Clade A lineage exhibited geographically distinct toxin profiles. The Malaysian strain (Western Pacific) produced Ovatoxin-k and Ovatoxin-j2 (this study) but the Japanese strains (s0743, s0752) produced the majority of Ovatoxin-a (Suzuki et al., 2012), and Brazilian strains (Western Atlantic) produced majority Ovatoxin-a and Ovatoxin-b (Nascimento et al., 2012; Tibiriçá et al., 2019). While the strains from the Mediterranean Sea produced a more diverse group of Ovatoxins comprised Ovatoxin-a, -b, -c, -d, and -e (Ciminello et al., 2010; Accoroni et al., 2011; Brissard et al., 2014; Tartaglione et al., 2017). It appeared that the toxigenic strains in Clade A are geographically widely distributed (Fig. 9), but the findings of distinct toxin profiles suggested that it is very unlikely that the wide distribution pattern of taxa in Clade A is attributed to recent dispersal event. In T5PRBos02, it could be the same toxic profile of their Cypriot *Ostreopsis* sp. CBA-C1012. This strain is identified as *O. fattorussoi* (Accoroni et al. 2016, Fig 7), therefore, it can have the same toxin profile in different species (ovata vs fattorussoi).

The production of Ostreocin-B and -D in the strain of *O. siamensis* in this study further confirmed that toxin production in *O. siamensis* is most likely species

specific. Previous study by Usami et al. (1995) revealed the production of palytoxin analogs with 70% of Ostreocin-D in a strain of *O. siamensis* collected from Okinawa, Japan. The species identity, however, could not be confirmed due to lack of morphology and molecular data. However, an *O. siamensis* strain S0587 from Okinawa produced exclusively Ostreocin-D (Sato et al., 2011, Suzuki et al., 2012). Later, Ostreocin-D, together with traces of Ostreocin-A and -B, were detected in the strains of *O. siamensis* from French Polynesia (Chomérat et al., 2020). These findings suggested that the production of Ostreocins is consistent in *O. siamensis* strains, but the toxin profiles may vary among geographically separated populations. To date, in the South China Sea, only one strain of *O. siamensis* from Malaysia was confirmed to produce Ostreocins. Although previous study by Tawong et al. (2014) had proven the toxicity of a *O. siamensis* strain from the Gulf of Thailand based on mouse bioassay, whether it produces Ostreocins with similar toxin profile to the Malaysian strain is an interesting topic to explore. It is also interesting to note that cells of *O. siamensis* collected during a bloom condition did not produce the toxins (Chomérat et al., 2020), suggesting that the toxin synthesis may be altered by its physiological conditions.

5. Conclusions

Two clades of *O*. cf. *ovata* have been recognized in the South China Sea, and each of them displays wide distribution in the world. *O. siamensis* proves to be similar to *O*. cf. *ovata* in morphology but may be separated by the ornamentation of thecal pores. *O. siamensis* has been recorded only in the Western Pacific to date but whether

it is present elsewhere will be interesting to investigate. *O*. cf. *ovata* clade A from the South China Sea is able to produce Ovatoxin-k and -j2, unlike those from elsewhere producing majority of Ovatoxin-a or -b. The production of Ostreocin in *O. siamensis* appears to be consistent but the different profiles may serve to differentiate geographically separated populations.

Acknowledgements

This work was supported by National Natural Science Foundation of China (42030404), the Scientific Research Foundation of Third Institute of Oceanography, MNR (No. 2020017), China-ASEAN Maritime Cooperation Fund, and the Ministry of Higher Education LRGS (LRGS/1/2020/UMT/01/1/3) and HICOE (IOES-2014C). We acknowledged technical support from Hwa Lin Yong, Nurin I. Mustapa and Zhaohe Luo for culture establishment. We thank Kenneth Mertens for helpful discussion and two anonymous reviewers for constructive suggestions.

References

Accoroni, S., Romagnoli, T., Colombo, F., Pennesi, C., Di Camillo, C.G., Marini, M., Battocchi, C., Ciminiello, P., Dell'Aversano, C., Iacovo, E.D., 2011. *Ostreopsis* cf. *ovata* bloom in the northern Adriatic Sea during summer 2009: ecology, molecular characterization and toxin profile. Mar. Pollut. Bull. 62(11), 2512–2519.

Accoroni, S., Romagnoli, T., Penna, A., Capellacci, S., Ciminiello, P., Dell'Aversano, C., Tartaglione, L., Abboud–Abi Saab, M., Giussani, V., Totti, C., 2016. *Ostreopsis fattorussoi* sp. nov. (Dinophyceae), a new benthic toxic *Ostreopsis* species from the eastern Mediterranean Sea. J. Phycol. 52(6), 1064–1084.

Adachi, M., Sako, Y., Ishida, Y., 1996. Analysis of *Alexandrium* (Dinophyceae) species using sequences of the 5.8S ribosomal DNA and internal transcribed spacer regions. J. Phycol. 32(3), 424–432.

Aligizaki, K., Nikolaidis, G., 2006. The presence of the potentially toxic genera *Ostreopsis* and *Coolia* (Dinophyceae) in the North Aegean Sea, Greece. Harmful Algae 5(6), 717–730.

Aligizaki, K., Katikou, P., Nikolaidis, G., Panou, A., 2008). First episode of shellfish contamination by palytoxin-like compounds from *Ostreopsis* species (Aegean Sea, Greece). Toxicon 51(3), 418–427.

Amzil, Z., Sibat, M., Chomerat, N., Grossel, H., Marco-Miralles, F., Lemee, R., Nezan, E., Sechet, V., 2012. Ovatoxin-a and palytoxin accumulation in seafood in relation to *Ostreopsis* cf. *ovata* blooms on the French Mediterranean

coast. Mar. Drugs 10(2), 477–496.

Balech, E., 1980. On the thecal morphology of dinoflagellates with special emphasis on circular and sulcal plates. Anales del Centro de Ciencias del Mar y Limnologia, Universidad Nacional Autonomia de Mexico 7, 57–68.

Berdalet, E., P.A. Tester, M. Chinain, S. Fraga, R. Lemée, W. Litaker, A. Penna, G. Usup, M. Vila, Zingone, A., 2017. Harmful algal blooms in benthic systems: Recent progress and future research. Oceanography 30(1), 36–45.

Besada, E., Loeblich, L., Loeblich, I., 1982. Observations on tropical, benthic dinoflagellates from ciguatera-endemic areas: *Coolia, Gambierdiscus*, and *Ostreopsis*. Bull. Mar. Sci. 32(3), 723–735.

Bire, R., Trotereau, S., Lemee, R., Delpont, C., Chabot, B., Aumond, Y., Krys, S., 2013. Occurrence of palytoxins in marine organisms from different trophic levels of the French Mediterranean coast harvested in 2009. Harmful Algae 28, 10–22.

Biré, R., Trotereau, S., Lemée, R., Oregioni, D., Delpont, C., Krys, S., Guérin, T., 2015. Hunt for Palytoxins in a Wide Variety of Marine Organisms Harvested in 2010 on the French Mediterranean Coast. Mar. Drugs, 13(8), 5425–5446

Boc, A., Diallo, A.B., Makarenkov, V., 2012. T-REX: a web server for inferring, validating and visualizing phylogenetic trees and networks. Nucleic Acids Res. 40(W1), W573–W579.

Brescianini C, Grillo C, Melchiorre N, Bertolotto R, Ferrari A, Vivaldi B, Icardi G, Gramaccioni L, Funari E, Scardala S., 2006. *Ostreopsis ovata* algal blooms

affecting human health in Genova, Italy, 2005 and 2006. Euro Surveill. 11(36), 3040.

Brissard, C., Herrenknecht, C., Séchet, V., Hervé, F., Pisapia, F., Harcouet, J., Lémée, R., Chomérat, N., Hess, P., Amzil, Z., 2014. Complex toxin profile of French Mediterranean *Ostreopsis* cf. *ovata* strains, seafood accumulation and ovatoxins prepurification. Mar. Drugs 12(5), 2851–2876.

Carnicer, O., Tunin-Ley, A., Andree, K.B., Turquet, J., Diogène, J., Fernández-Tejedor, M., 2015. Contribution to the genus *Ostreopsis* in Reunion Island (Indian Ocean): molecular, morphologic and toxicity characterization. Cryptogamie Algol. 36(1), 101–119.

Chang, F., Shimizu, Y., Hay, B., Stewart, R., Mackay, G., Tasker, R., 2000. Three recently recorded *Ostreopsis* spp. (Dinophyceae) in New Zealand: temporal and regional distribution in the upper North Island from 1995 to 1997. N. Z. J. Mar. Freshwat. Res. 34(1), 29–39.

Chomérat, N., Bilien, G., Derrien, A., Henry, K., Ung, A., Viallon, J., Darius, H.T., Mahana iti Gatti, C., Roué, M., Hervé, F., Réveillon, D., Amzil, Z., Chinain, M., 2019. *Ostreopsis lenticularis* Y. Fukuyo (Dinophyceae, Gonyaulacales) from French Polynesia (South Pacific Ocean): A revisit of its morphology, molecular phylogeny and toxicity. Harmful Algae 84, 95–111.

Chomérat, N., Bilien, G., Viallon, J., Hervé, F., Réveillon, D., Henry, K., Zubia, M., Vieira, C., Ung, A., Mahana iti Gatti, Roué, M., Derrien, A., Amzil, Z., Darius, H.T., Chinain, M., 2020. Taxonomy and toxicity of a bloom-forming *Ostreopsis*

species (Dinophyceae, Gonyaulacales) in Tahiti island (South Pacific Ocean): one step further towards resolving the identity of *O. siamensis*. Harmful Algae 98, 101888.

Ciminiello, P., Dell'Aversano, C., Iacovo, E.D., Fattorusso, E., Forino, M., Grauso, L., Tartaglione, L., Guerrini, F., Pistocchi, R., 2010. Complex palytoxin-like profile of *Ostreopsis ovata*. Identification of four new ovatoxins by high-resolution liquid chromatography/mass spectrometry. Rapid Commun. Mass Sp. 24(18), 2735–2744.

Ciminiello, P., Dell'Aversano, C., Iacovo, E. D., Fattorusso, E., Forino, M., Tartaglione, L., Benedettini,G., Onorari, M., Serena, F., Battocchi, C., Casabianca, S., Penna, A., 2014. First finding of *Ostreopsis* cf. *ovata* toxins in marine aerosols. Environ. Sci. Tech., 48(6), 3532–3540.

Daugbjerg, N., Hansen, G., Larsen, J., Moestrup, Ø., 2000. Phylogeny of some of the major genera of dinoflagellates based on ultrastructure and partial LSU rDNA sequence data, including the erection of three new genera of unarmoured dinoflagellates. Phycologia 39(4), 302–317.

David, H., Laza-Martínez, A., Miguel, I., Orive, E., 2013. *Ostreopsis* cf. *siamensis* and *Ostreopsis* cf. *ovata* from the Atlantic Iberian Peninsula: Morphological and phylogenetic characterization. Harmful Algae 30, 44–55.

Faust, M.A., Morton, S.L., 1995. Morphology and ecology of the marine dinoflagellate *Ostreopsis labens* sp. nov. (Dinophyceae). J. Phycol. 31(3), 456–463.

Faust, M.A., Morton, S.L., Quod, J.P., 1996. Further SEM study of marine dinoflagellates: the genus *Ostreopsis* (Dinophyceae). J. Phycol. 32(6), 1053–1065.

Faust, M. A.,1999. Three new *Ostreopsis* species (Dinophyceae): *O. marinus* sp. nov., *O. belizeanus* sp. nov., and *O. caribbeanus* sp. nov. Phycologia 38(2), 92–99.

Fensome, R.A., Taylor, F.J.R., Norris, G., Sarjeant, W.A.S., Wharton, D.I., Williams, G.L., 1993. A classification of fossil and living dinoflagellates. Micropaleontology Special Publication 7, 1–245.

Fritz, L., Triemer, R., 1985. A rapid simple technique utilizing calcofluor white M2R for the visualization of dinoflagellate thecal plates. J. Phycol. 21(4), 662–664.

Fu, Z., Piumsomboon, A., Punnarak, P., Uttayarnmanee P., Leaw C.P., Lim, P.T., Wang, A., Gu, H., 2021. Diversity and distribution of harmful microalgae in the Gulf of Thailand assessed by DNA metabarcoding. Harmful Algae 106, 102063.

Fukuyo, Y., 1981. Taxonomical study on benthic dinoflagellates collected in coral reefs. Bull. Jpn. Soc. Sci. Fish. 47(8), 967–978.

Giussani, V., Asnaghi, V., Pedroncini, A., Chiantore, M., 2017. Management of harmful benthic dinoflagellates requires targeted sampling methods and alarm thresholds. Harmful Algae 68, 97–104.

Gladan, N.Ž., Arapov, J., Casabianca, S., Penna, A., Honsell, G., Brovedani, V., Pelin, M., Tartaglione, L., Sosa, S., Dell'Aversano, C., Tubaro, A., Žuljević, A., Grbec, B., Čavar, M., Bužančić, M., Bakrač, A., Skejić, S., 2019. Massive occurrence of the harmful benthic dinoflagellate *Ostreopsis* cf. *ovata* in the Eastern Adriatic

Sea. Toxins 11(5), 300. doi:10.3390/toxins11050300.

García-Altares, M., Tartaglione, L., Dell'Aversano, C., Carnicer, O., de la Iglesia, P., Forino, M., Diogène, J., Ciminiello, P., 2015. The novel ovatoxin-g and isobaric palytoxin (so far referred to as putative palytoxin) from *Ostreopsis* cf. *ovata* (NW Mediterranean Sea): structural insights by LC-high resolution MS n. Anal. Bioanal. Chem., 407(4), 1191–1204.

Gomez, F., Qiu, D., Lin, S., 2017. Morphological and molecular characterization of the toxic dinoflagellate *Ostreopsis* cf. *ovata* (Gonyaulacales: Dinophyceae) from Brazil (South Atlantic Ocean). Rev. Biol. Trop. 65(3), 1022–1032.

Guillard, R.R.L., Ryther, J.H., 1962. Studies of marine planktonic diatoms. I. *Cyclotella nana* Hustedt and *Detonula confervacea* Cleve. Can. J. Microbiol. 8, 229–239.

Guiry, M.D., Guiry, G.M. 2021. *AlgaeBase*. World-wide electronic publication, National University of Ireland, Galway. http://www.algaebase.org; searched on 07 September 2021.

Hall, T.A., 1999. BioEdit: a user-friendly biological sequence alignment editor and analysis program for Windows 95/98/NT, In: Series, N.A.S. (Ed.), pp. 95–98.

Honsell, G., Bortoli, M. De, Boscolo, S., Dell'Aversano, C., Battocchi, C., Fontanive, G., Penna, A., Berti, F., Sosa, S., Yasumoto, T., Ciminiello, P., Poli, M., Tubaro, A. 2011. Harmful dinoflagellate *Ostreopsis* cf. *ovata* Fukuyo: Detection of Ovatoxins in field samples and cell immunolocalization using antipalytoxin antibodies. Environ. Sci. Technol. 45 (16), 7051–7059.

Jauzein, C., Açaf, L., Accoroni, S., Asnaghi, V., Fricke, A., Hachani, M. A., Saab, M., Chiantore, M., Mangialajo, L., Totti, C., Zaghmouri, I., Lemée, R., 2018. Optimization of sampling, cell collection and counting for the monitoring of benthic harmful algal blooms: Application to *Ostreopsis* spp. blooms in the Mediterranean Sea. Ecol. Indic. 91, 116–127.

Kang, N.S., Jeong, H.J., Lee, S.Y., Lim, A.S., Lee, M.J., Kim, H.S., Yih, W., 2013. Morphology and molecular characterization of the epiphytic benthic dinoflagellate *Ostreopsis* cf. *ovata* in the temperate waters off Jeju Island, Korea. Harmful Algae 27, 98–112.

Katoh, K., Standley, D.M., 2013. MAFFT multiple sequence alignment software version 7: improvements in performance and usability. Mol. Biol. Evol. 30(4), 772–780.

Leaw, C.P., Lim, P.T., Ahmad, A., Usup, G., 2001. Genetic diversity of *Ostreopsis ovata* (Dinophyceae) from Malaysia. Mar. Biotechnol. 3(3), 246–255.

Lee, L. K., Lim, Z. F., Gu, H., Chan, L. L., Litaker, R. W., Tester, P. A., Leaw, C. P., Lim, P. T., 2020. Effects of substratum and depth on benthic harmful dinoflagellate assemblages. Sci. Rep. 10(1), 1–14.

Medina-Pérez, N. I., Dall'Osto, M., Decesari, S., Paglione, M., Moyano, E., Berdalet, E., 2020. Aerosol toxins emitted by harmful algal blooms susceptible to complex air–sea interactions. Environ. Sci. Tech. 55(1), 468–477.

Mohammad-Noor, N., Daugbjerg, N., Moestrup, Ø., Anton, A., 2007. Marine epibenthic dinoflagellates from Malaysia--A study of live cultures and preserved

samples based on light and scanning electron microscopy. Nord. J. Bot. 24(6), 629–690.

Nascimento, S.M., Corrêa, E.V., Menezes, M., Varela, D., Paredes, J., Morris, S., 2012. Growth and toxin profile of *Ostreopsis* cf. *ovata* (Dinophyta) from Rio de Janeiro, Brazil. Harmful Algae 13, 1–9.

Nguyen-Ngoc, L., Doan-Nhu, H., Larsen, J., Phan-Tan, L., Nguyen, X.-V., Lundholm, N., Van Chu, T., Huynh-Thi, D.N. 2021. Morphological and genetic analyses of *Ostreopsis* (Dinophyceae, Gonyaulacales, Ostreopsidaceae) species from Vietnamese waters with a re-description of the type species, *O. siamensis*. J. Phycol., 57: 1059–1083.

Nylander, J.A., Wilgenbusch, J.C., Warren, D.L., Swofford, D.L., 2008. AWTY (are we there yet?): a system for graphical exploration of MCMC convergence in Bayesian phylogenetics. Bioinformatics 24(4), 581–583.

Parsons, M. L., Aligizaki, K., Bottein, M. Y. D., Fraga, S., Morton, S. L., Penna, A., & Rhodes, L., 2012. *Gambierdiscus* and *Ostreopsis*: reassessment of the state of knowledge of their taxonomy, geography, ecophysiology, and toxicology. Harmful Algae 14, 107–129.

Pavaux, A. S., Berdalet, E., & Lemée, R. 2020. Chemical ecology of the benthic dinoflagellate genus *Ostreopsis*: review of progress and future directions. Front Mar Sci., 7, 498.

Penna, A., Fraga, S., Battocchi, C., Casabianca, S., Giacobbe, M.G., Riobó, P., Vernesi, C., 2010. A phylogeographical study of the toxic benthic dinoflagellate

genus *Ostreopsis* Schmidt. J. Biogeogr. 37(5), 830–841.

Penna, A., Vila, M., Fraga, S., Giacobbe, M.G., Andreoni, F., Riobó, P., Vernesi, C., 2005. Characterization of *Ostreopsis* and *Coolia* (Dinophyceae) isolates in the Western Mediterranean sea based on morphology, toxicity and Internal Transcribed Spacer 5.8S rDNA sequences. J. Phycol. 41(1), 212–225.

Posada, D., 2008. jModelTest: phylogenetic model averaging. Mol. Biol. Evol. 25(7), 1253–1256.

Quod, J. P. (1994). *Ostreopsis mascarenensis* sp. nov. (Dinophyceae), dinoflagellé toxique associé à la ciguatera dans l'océan Indien. Cryptogamie Algol. 15(4), 243–251.

Ramos, V., Vasconcelos, V., 2010. Palytoxin and analogs: biological and ecological effects. Mar. Drugs 8(7), 2021–2037.

Rhodes, L. 2011. World-wide occurrence of the toxic dinoflagellate genus *Ostreopsis* Schmidt. Toxicon 57(3), 400–407.

Rhodes, L. L., Smith, K. F., Verma, A., Murray, S., Harwood, D. T., Trnski, T., 2017. The dinoflagellate genera *Gambierdiscus* and *Ostreopsis* from subtropical Raoul Island and North Meyer Island, Kermadec Islands. New Zeal. J. Mar. Fresh. 51(4), 490–504.

Ronquist, F., Huelsenbeck, J.P., 2003. MrBayes 3: Bayesian phylogenetic inference under mixed models. Bioinformatics 19(12), 1572–1574.

Sato, S., Nishimura, T., Uehara, K., Sakanari, H., Tawong, W., Hariganeya, N., Smith, K., Rhodes, L., Yasumoto, T., Taira, Y., 2011. Phylogeography of *Ostreopsis*

along west Pacific coast, with special reference to a novel clade from Japan. PloS one 6(12), e27983.

Schmidt, J., 1901. Flora of Koh Chang: contributions to the knowledge of the vegetation in the Gulf of Siam. Peridiniales. Botanisk Tidsskrift 24, 212–221.

Spurr, R., 1969. A low-viscosity epoxy resin embedding medium for electron microscopy. J. Ultras. Res. 26, 31–43.

Stamatakis, A., 2006. RAxML-VI-HPC: maximum likelihood-based phylogenetic analyses with thousands of taxa and mixed models. Bioinformatics 22(21), 2688–2690.

Suzuki, T., Watanabe, R., Uchida, H., Matsushima, R., Nagai, H., Yasumoto, T., Yoshimatsu, T., Sato, S., Adachi, M., 2012. LC-MS/MS analysis of novel ovatoxin isomers in several *Ostreopsis* strains collected in Japan. Harmful Algae 20, 81–91.

Swofford, D.L., 2002. PAUP 4.0b10: Phylogenetic analysis using parsimony, Sinauer Associates, Sunderland, MA, U.S.A.

Tartaglione, L., Dello Iacovo, E., Mazzeo, A., Casabianca, S., Ciminiello, P., Penna, A., Dell'Aversano, C., 2017. Variability in toxin profiles of the Mediterranean *Ostreopsis* cf. *ovata* and in structural features of the produced ovatoxins. Environ. Sci. Technol. 51(23), 13920–13928.

Tawong, W., Nishimura, T., Sakanari, H., Sato, S., Yamaguchi, H., Adachi, M., 2014. Distribution and molecular phylogeny of the dinoflagellate genus *Ostreopsis* in Thailand. Harmful Algae 37, 160–171.

Tibiriçá, C.E.J.A., Leite, I.P., Batista, T.V.V., Fernandes, L.F., Chomérat, N., Hervé, F., Hess, P., Mafra, L.L., 2019. *Ostreopsis* cf. *ovata* bloom in Currais, Brazil: Phylogeny, toxin profile and contamination of mussels and marine plastic litter. Toxins 11(8), 446.

Tubaro, A., Durando, P., Del Favero, G., Ansaldi, F., Icardi, G., Deeds, J. R., Sosa, S., 2011. Case definitions for human poisonings postulated to palytoxins exposure. Toxicon, 57(3), 478–495.

Tognetto, L., Bellato, S., Moro, I., Andreoli, C., 1995. Occurrence of *Ostreopsis ovata* (Dinophyceae) in the Tyrrhenian Sea during summer 1994. Bot. Mar. 38(1–6), 291–296.

Totti, C., Accoroni, S., Cerino, F., Cucchiari, E., Romagnoli, T., 2010. *Ostreopsis ovata* bloom along the Conero Riviera (northern Adriatic Sea): relationships with environmental conditions and substrata. Harmful Algae 9(2), 233–239.

Verma, A., Hoppenrath, M., Harwood, T., Brett, S., Rhodes, L., Murray, S., 2016. Molecular phylogeny, morphology and toxigenicity of *Ostreopsis* cf. *siamensis* (Dinophyceae) from temperate south-east Australia. Phycol. Res. 64(3), 146–159.

Vila, M., Abós-Herràndiz, R., Isern-Fontanet, J., Àlvarez, J., Berdalet, E., 2016. Establishing the link between *Ostreopsis* cf. *ovata* blooms and human health impacts using ecology and epidemiology. Sci. Mar. 80(S1), 107–115.

Yong, H. L., Mustapa, N. I., Lee, L. K., Lim, Z. F., Tan, T. H., Usup, G., Gu, H., Litaker, R.W., Tester P. A., Lim P. T., Leaw, C. P., 2018. Habitat complexity

affects benthic harmful dinoflagellate assemblages in the fringing reef of Rawa Island, Malaysia. Harmful Algae, 78, 56–68.

Zhang, H., Lu, S., Li, Y., Cen, J., Wang, H., Li, Q., Nie, X., 2018. Morphology and molecular phylogeny of *Ostreopsis* cf. *ovata* and *O. lenticularis* (Dinophyceae) from Hainan Island, South China Sea. Phycol. Res. 66(1), 3–14.

Figure captions

Fig. 1. Map of sampling stations in the South China Sea. Map of sampling stations in the South China Sea. 1: Weizhou, Beihai, China; 2: Changjiang, Hainan, China; 3, 4: Sanya, Hainan, China; 5: Mak, Trat, Thailand; 6: Rawa, Terengganu, Malaysia.

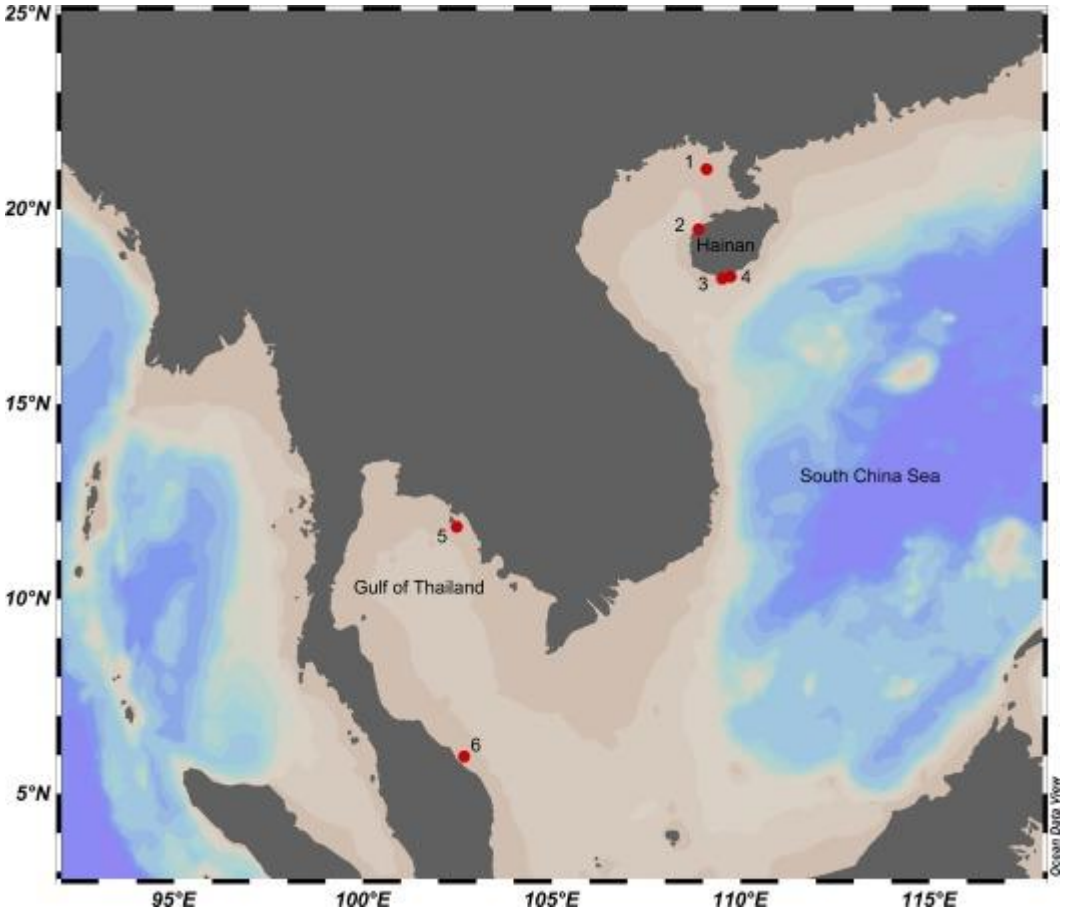

Fig. 2. Light and epifluorescence micrographs of cells of *Ostreopsis* cf. *ovata* strain TIO897. (A, B) Living cells; (C) Autofluorescence image of a cell showing numerous radially arranged chloroplasts (C); (D) Epifluorescence image of a SYBR Green-stained cell showing a spherical nucleus (N) in the posterior end; (E, F) Calcoflour-stained cells.

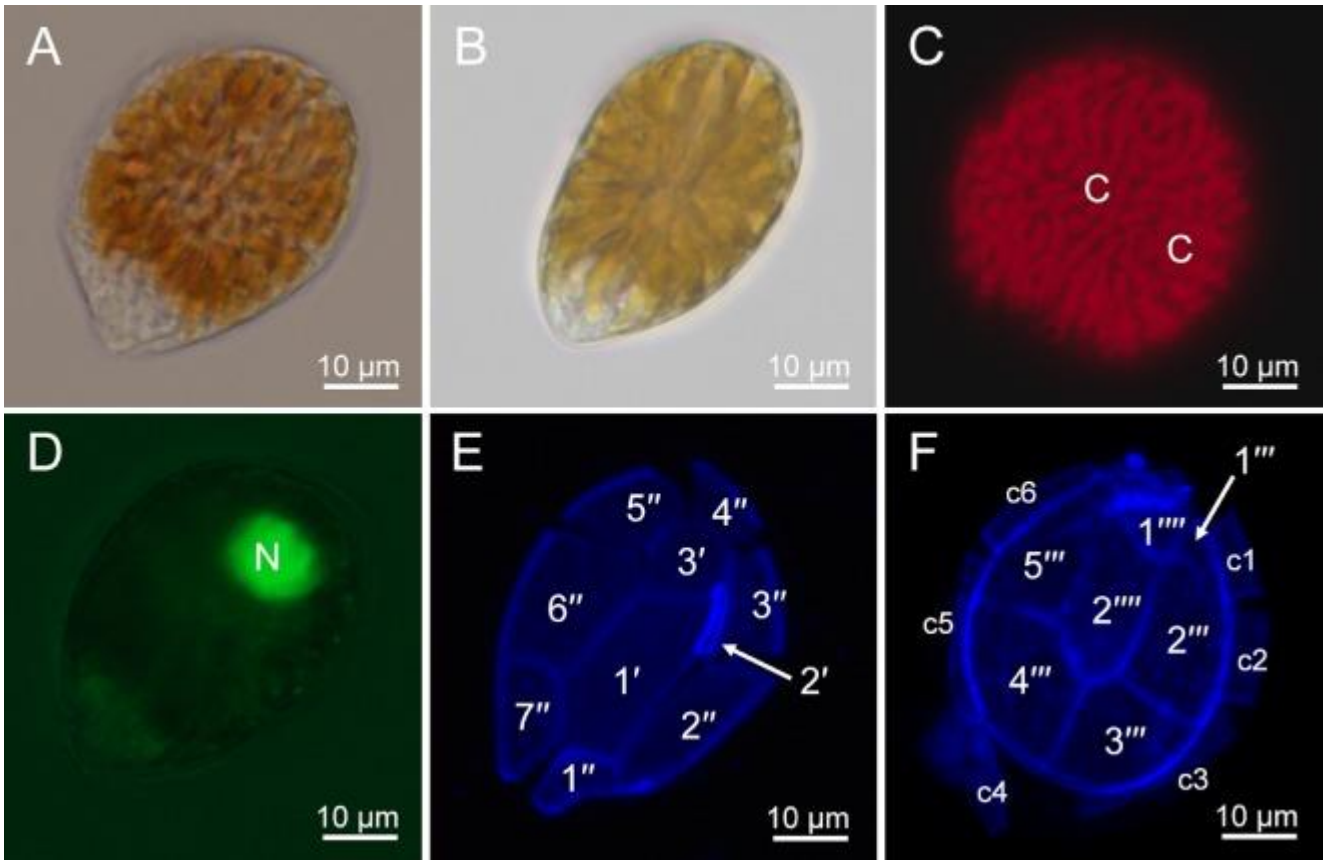

Fig. 3. Scanning electron micrographs of vegetative cells of *Ostreopsis* cf. *ovata* strain TIO897. (A) Ventral view. (B) Apical view showing two apical plates (1′, 3′), and seven precingular plates (1″ – 7″). (C) Antapical view showing four postcingular plates (2‴ – 5‴) and two antapical plates (1⁗, 2⁗). (D) Ventral area of the sulcus showing anterior sulcal plate (Sa), right sulcal plates (Sda, Sdp), left sulcal plate (Ssa, Ssp), and posterior sulcal plate (Sp). (E, F) Detail of apical pore and surrounding plates.

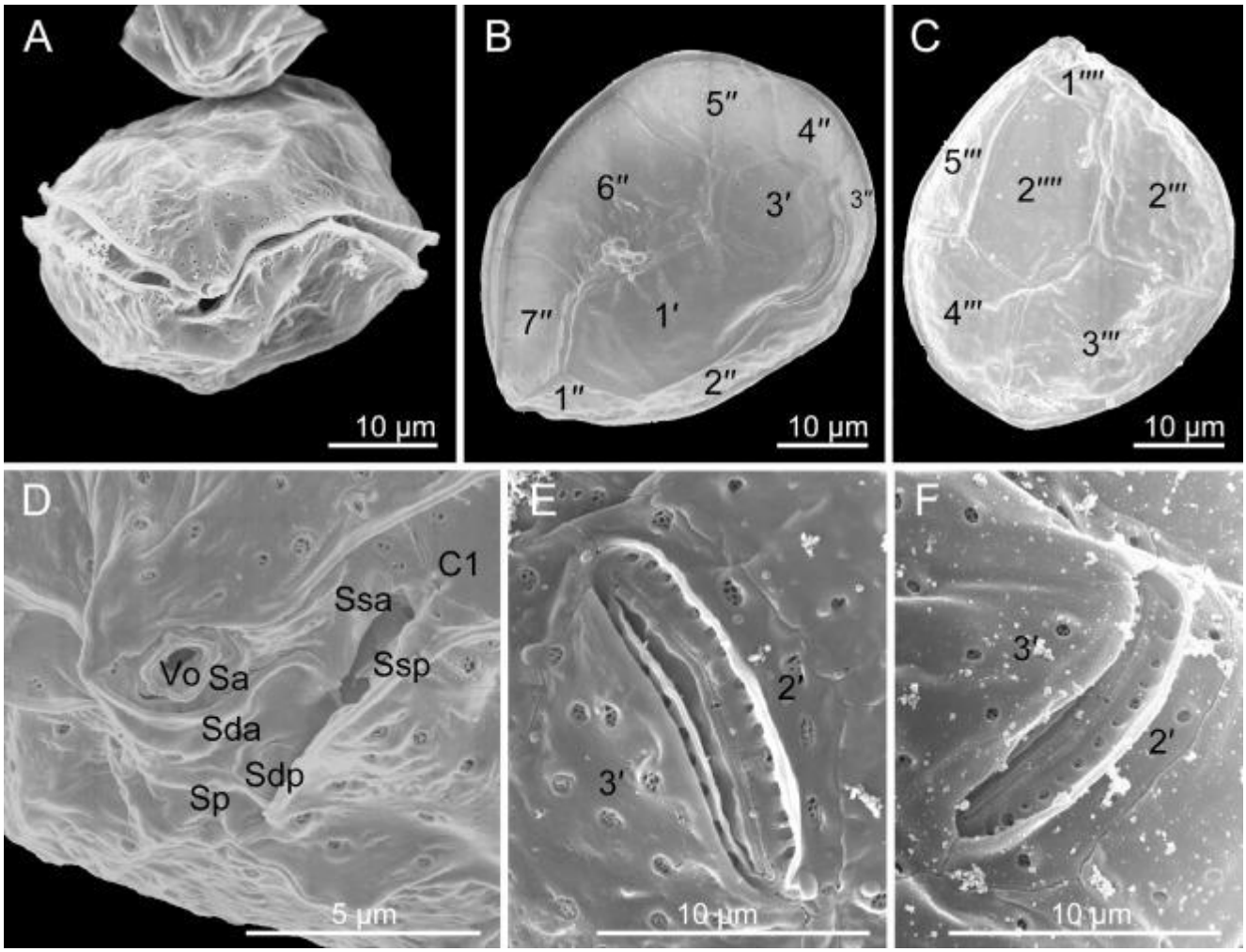

Fig. 4. Transmission electron micrographs of vegetative cells of *Ostreopsis* cf. *ovata* strain TIO897. (A) Longitudinal sections through the cell showing a large nucleus (N), starch grains (S), and lipid bodies (L). (B) Transverse section through cell showing radial chloroplasts. (C) Closeup of chloroplasts (C), starch grains (S), and lipid bodies (L). (D) The chloroplast showing the thylakoids grouped in twos or threes to form lamellae, and a trichocyst (t). (E) Detail of the nucleus showing a nucleolus (n). (F) The mucocyst canal (MC) surrounded by many mucocysts (M).

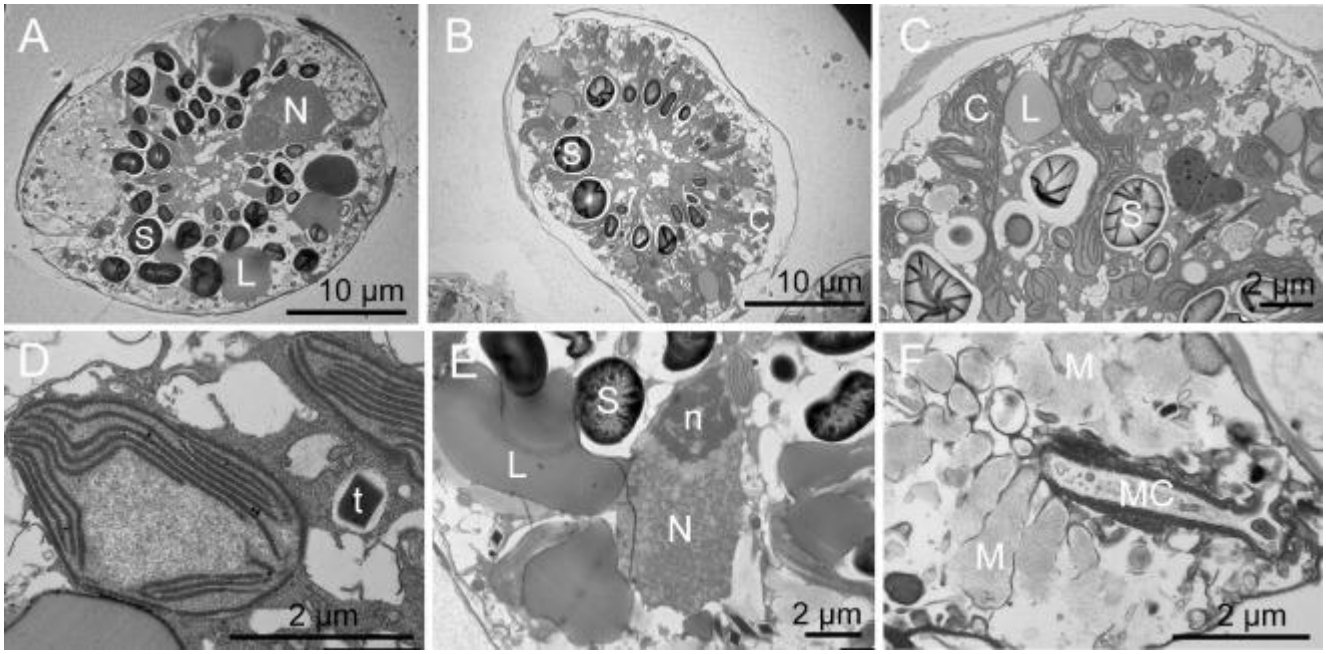

Fig. 5. Scanning electron micrographs of vegetative cells of *Ostreopsis siamensis* strain T10PRBost04. (A) Ventral view; (B) Apical view showing two apical plates (1′, 3′), and seven precingular plates (1″ – 7″); (C) Detail of apical pore and surrounding plates. (D) Antapical view showing five postcingular plates (1‴ – 5‴) and two antapical plates (1⁗, 2⁗); (E) Ventral area of the sulcus showing anterior sulcal plate (Sa), right sulcal plates (Sda), left sulcal plate (Ssa, Ssp), and posterior sulcal plate (Sp) and the first postcingular (1‴) and antapical plates (1⁗). (F) The cingulum showing six cingular plates.

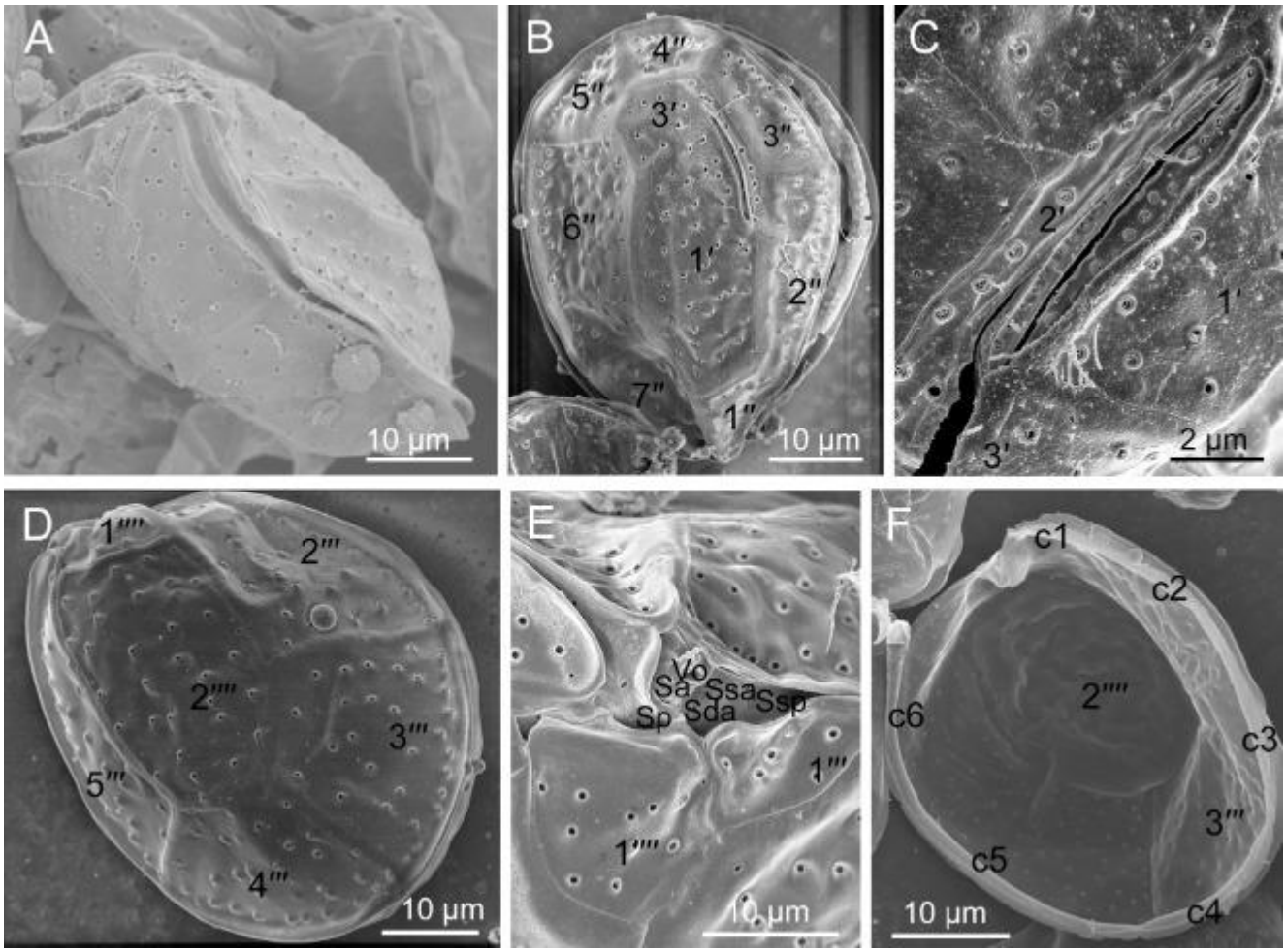

Fig. 6. Phylogenetic tree inferred from maximum likelihood (ML) based on the *Ostreopsis* LSU rDNA (D1–D3) sequences. Nodal labels in red indicate new strains and sequences obtained in this study. Branch lengths are drawn to scale, with the scale bar indicating the number of nucleotide substitutions per site. The dashed line indicates half length. Nodal supports are bootstrap values of ML and Bayesian posterior probabilities (PP). Only ML values >50% and PP >0.8 are shown. Asterisk indicates ML bootstrap support value of 100% and a PP of 1.0.

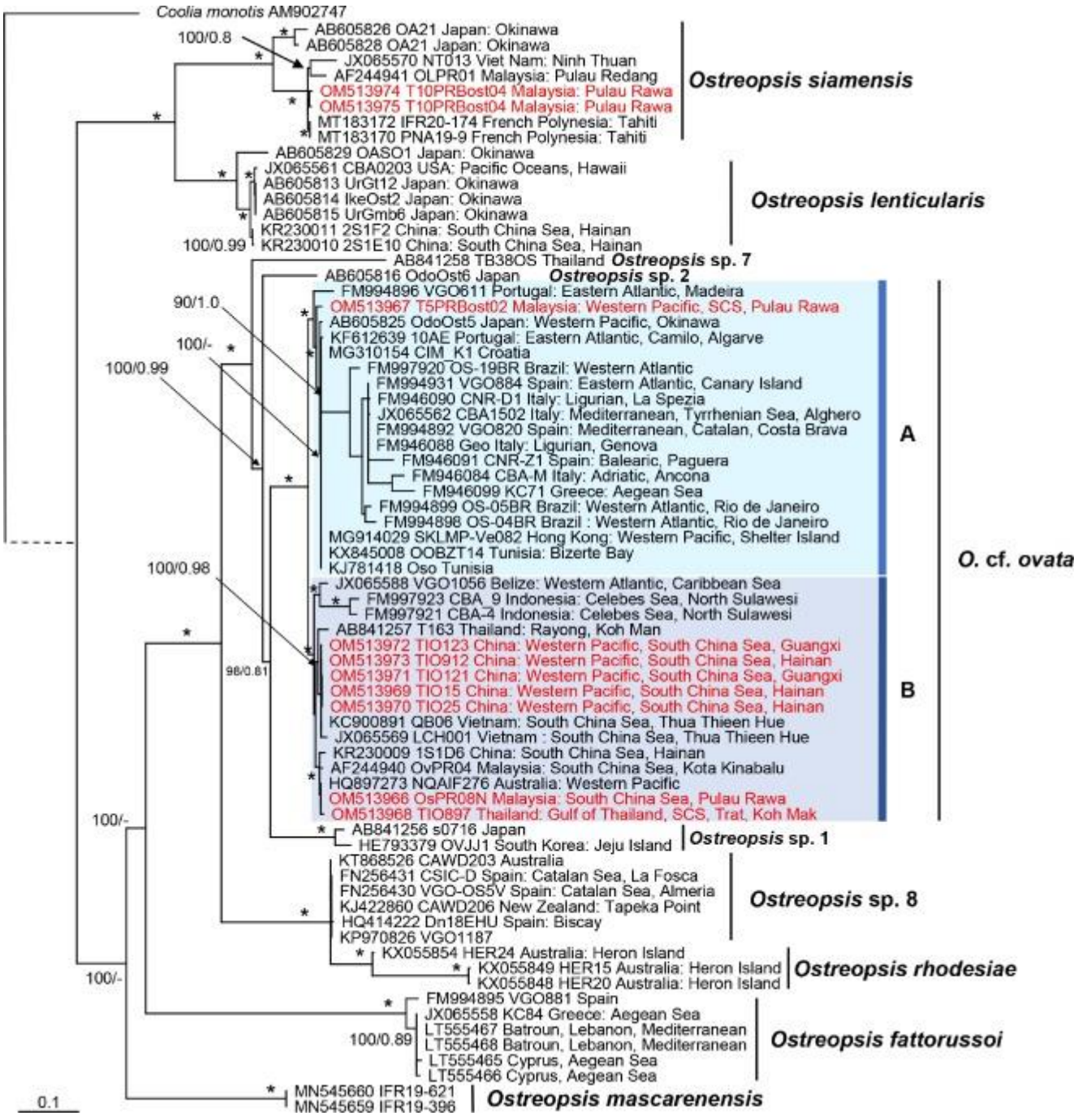
Coolia monotis AM902747
AB605826 OA21 Japan: Okinawa
AB605828 OA21 Japan: Okinawa
JX065570 NT013 Viet Nam: Ninh Thuan
AF244941 OLPR01 Malaysia: Pulau Redang
OM513974 T10PRBost04 Malaysia: Pulau Rawa
OM513975 T10PRBost04 Malaysia: Pulau Rawa
MT183172 IFR20-174 French Polynesia: Tahiti
MT183170 PNA19-9 French Polynesia: Tahiti
Ostreopsis siamensis
AB605829 OASO1 Japan: Okinawa
JX065561 CBA0203 USA: Pacific Oceans, Hawaii
AB605813 UrGt12 Japan: Okinawa
AB605814 IkeOst2 Japan: Okinawa
AB605815 UrGmb6 Japan: Okinawa
KR230011 2S1F2 China: South China Sea, Hainan
KR230010 2S1E10 China: South China Sea, Hainan
Ostreopsis lenticularis
AB841258 TB38OS Thailand Ostreopsis sp. 7
AB605816 OdoOst6 Japan Ostreopsis sp. 2
FM994896 VGO611 Portugal: Eastern Atlantic, Madeira
OM513967 T5PRBost02 Malaysia: Western Pacific, SCS, Pulau Rawa
AB605825 OdoOst5 Japan: Western Pacific, Okinawa
KF612639 10AE Portugal: Eastern Atlantic, Camilo, Algarve
MG310154 CIM_K1 Croatia
FM997920 OS-19BR Brazil: Western Atlantic
FM994931 VGO884 Spain: Eastern Atlantic, Canary Island
FM946090 CNR-D1 Italy: Ligurian, La Spezia
JX065562 CBA1502 Italy: Mediterranean, Tyrrhenian Sea, Alghero
FM994892 VGO820 Spain: Mediterranean, Catalan, Costa Brava
FM946088 Geo Italy: Ligurian, Genova
FM946091 CNR-Z1 Spain: Balearic, Paguera
FM946084 CBA-M Italy: Adriatic, Ancona
FM946099 KC71 Greece: Aegean Sea
FM994899 OS-05BR Brazil: Western Atlantic, Rio de Janeiro
FM994898 OS-04BR Brazil : Western Atlantic, Rio de Janeiro
MG914029 SKLMP-Ve082 Hong Kong: Western Pacific, Shelter Island
KX845008 OOBZT14 Tunisia: Bizerte Bay
KJ781418 Oso Tunisia
A
JX065588 VGO1056 Belize: Western Atlantic, Caribbean Sea
FM997923 CBA_9 Indonesia: Celebes Sea, North Sulawesi
FM997921 CBA_4 Indonesia: Celebes Sea, North Sulawesi
AB841257 T163 Thailand: Rayong, Koh Man
OM513972 TIO123 China: Western Pacific, South China Sea, Guangxi
OM513973 TIO912 China: Western Pacific, South China Sea, Hainan
OM513971 TIO121 China: Western Pacific, South China Sea, Guangxi
OM513969 TIO15 China: Western Pacific, South China Sea, Hainan
OM513970 TIO25 China: Western Pacific, South China Sea, Hainan
KC900891 QB06 Vietnam: South China Sea, Thua Thieen Hue
JX065569 LCH001 Vietnam : South China Sea, Thua Thieen Hue
KR230009 1S1D6 China: South China Sea, Hainan
AF244940 OvPR04 Malaysia: South China Sea, Kota Kinabalu
HQ897273 NQAIF276 Australia: Western Pacific
OM513966 OsPR08N Malaysia: South China Sea, Pulau Rawa
OM513968 TIO897 Thailand: Gulf of Thailand, SCS, Trat, Koh Mak
B
O. cf. ovata
AB841256 s0716 Japan
HE793379 OVJJ1 South Korea: Jeju Island
Ostreopsis sp. 1
KT868526 CAWD203 Australia
FN256431 CSIC-D Spain: Catalan Sea, La Fosca
FN256430 VGO-OS5V Spain: Catalan Sea, Almeria
KJ422860 CAWD206 New Zealand: Tapeka Point
HQ414222 Dn18EHU Spain: Biscay
KP970826 VGO1187
Ostreopsis sp. 8
KX055854 HER24 Australia: Heron Island
KX055849 HER15 Australia: Heron Island
KX055848 HER20 Australia: Heron Island
Ostreopsis rhodesiae
FM994895 VGO881 Spain
JX065558 KC84 Greece: Aegean Sea
LT555467 Batroun, Lebanon, Mediterranean
LT555468 Batroun, Lebanon, Mediterranean
LT555465 Cyprus, Aegean Sea
LT555466 Cyprus, Aegean Sea
Ostreopsis fattorussoi
MN545660 IFR19-621
MN545659 IFR19-396
Ostreopsis mascarenensis
100/0.8
100/0.99
90/1.0
100/-
100/0.99
100/0.98
98/0.81
100/-
100/-
100/0.89
0.1

Fig. 7. Phylogenetic tree inferred from maximum likelihood (ML) based on the internal transcribed spacer (ITS) region sequences of *Ostreopsis* species. Nodal labels in red indicate new strains and sequences obtained in this study. Branch lengths are drawn to scale, with the scale bar indicating the number of nucleotide substitutions per site. The dashed line indicates half length. Nodal supports are bootstrap values of ML and Bayesian posterior probabilities (PP). Only ML values >50% and PP >0.8 are shown. Asterisk indicates ML bootstrap support value of 100% and a PP of 1.0.

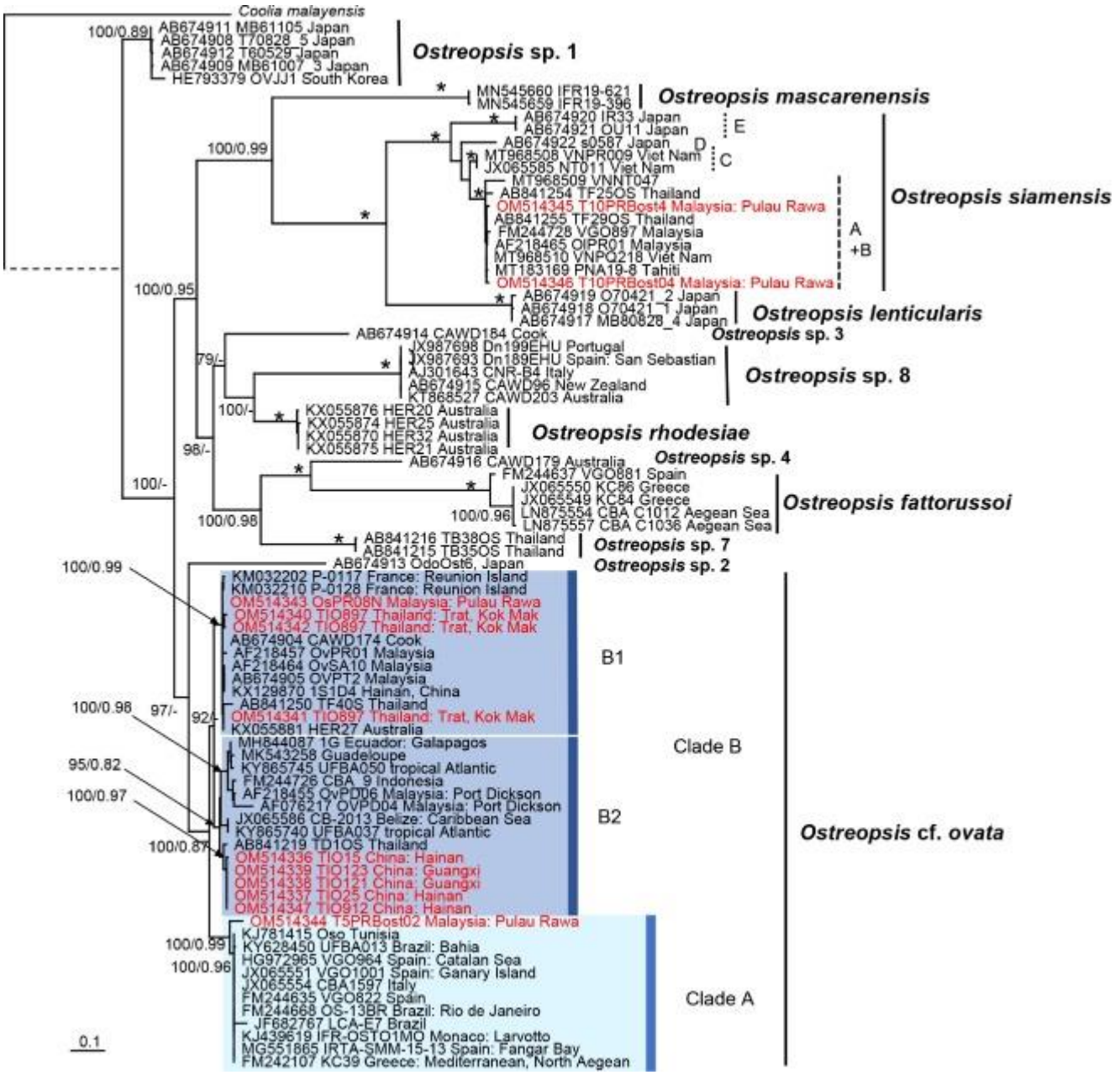
Coolia malayensis
AB674911 MB61105 Japan
AB674908 T70828_5 Japan
AB674912 T60529 Japan
AB674909 MB61007_3 Japan
HE793379 OVJJ1 South Korea
Ostreopsis sp. 1
MN545660 IFR19-621
MN545659 IFR19-396
Ostreopsis mascarenensis
AB674920 IR33 Japan
AB674921 OU11 Japan
AB674922 s0587 Japan
MT968508 VNPR009 Viet Nam
JX065585 NT011 Viet Nam
MT968509 VNNT047
AB841254 TF25OS Thailand
OM514345 T10PRBost4 Malaysia: Pulau Rawa
AB841255 TF29OS Thailand
FM244728 VGO897 Malaysia
AF218465 OlPR01 Malaysia
MT968510 VNPQ218 Viet Nam
MT183169 PNA19-8 Tahiti
OM514346 T10PRBost04 Malaysia: Pulau Rawa
E
D
C
A
+B
Ostreopsis siamensis
AB674919 O70421_2 Japan
AB674918 O70421_1 Japan
AB674917 MB80828_4 Japan
Ostreopsis lenticularis
AB674914 CAWD184 Cook
Ostreopsis sp. 3
JX987698 Dn199EHU Portugal
JX987693 Dn189EHU Spain: San Sebastian
AJ301643 CNR-B4 Italy
AB674915 CAWD96 New Zealand
KT868527 CAWD203 Australia
Ostreopsis sp. 8
KX055876 HER20 Australia
KX055874 HER25 Australia
KX055870 HER32 Australia
KX055875 HER21 Australia
Ostreopsis rhodesiae
AB674916 CAWD179 Australia
Ostreopsis sp. 4
FM244637 VGO881 Spain
JX065550 KC86 Greece
JX065549 KC84 Greece
LN875554 CBA C1012 Aegean Sea
LN875557 CBA C1036 Aegean Sea
Ostreopsis fattorussoi
AB841216 TB38OS Thailand
AB841215 TB35OS Thailand
Ostreopsis sp. 7
AB674913 OdoOst6, Japan
Ostreopsis sp. 2
KM032202 P-0117 France: Reunion Island
KM032210 P-0128 France: Reunion Island
OM514343 OsPR08N Malaysia: Pulau Rawa
OM514340 TIO897 Thailand: Trat, Kok Mak
OM514342 TIO897 Thailand: Trat, Kok Mak
AB674904 CAWD174 Cook
AF218457 OvPR01 Malaysia
AF218464 OvSA10 Malaysia
AB674905 OVPT2 Malaysia
KX129870 1S1D4 Hainan, China
AB841250 TF40S Thailand
OM514341 TIO897 Thailand: Trat, Kok Mak
KX055881 HER27 Australia
B1
MH844087 1G Ecuador: Galapagos
MK543258 Guadeloupe
KY865745 UFBA050 tropical Atlantic
FM244726 CBA_9 Indonesia
AF218455 OvPD06 Malaysia: Port Dickson
AF076217 OVPD04 Malaysia: Port Dickson
JX065586 CB-2013 Belize: Caribbean Sea
KY865740 UFBA037 tropical Atlantic
AB841219 TD1OS Thailand
OM514336 TIO15 China: Hainan
OM514339 TIO123 China: Guangxi
OM514338 TIO121 China: Guangxi
OM514337 TIO25 China: Hainan
OM514347 TIO912 China: Hainan
B2
Clade B
OM514344 T5PRBost02 Malaysia: Pulau Rawa
KJ781415 Oso Tunisia
KY628450 UFBA013 Brazil: Bahia
HG972965 VGO964 Spain: Catalan Sea
JX065551 VGO1001 Spain: Ganary Island
JX065554 CBA1597 Italy
FM244635 VGO822 Spain
FM244668 OS-13BR Brazil: Rio de Janeiro
JF682767 LCA-E7 Brazil
KJ439619 IFR-OSTO1MO Monaco: Larvotto
MG551865 IRTA-SMM-15-13 Spain: Fangar Bay
FM242107 KC39 Greece: Mediterranean, North Aegean
Clade A
Ostreopsis cf. ovata
100/0.89
100/0.99
100/0.95
79/-
100/-
98/-
100/-
100/0.98
100/0.96
100/0.99
100/0.96
97/-
92/-
95/0.82
100/0.97
100/0.87
100/0.99
100/0.96
0.1

Fig. 8. A world map showing distribution of *Ostreopsis* cf. *ovata* clades A (green circles) and B (yellow circles).